Whitmore, J.H. 2023. Can sandstone cross-bed dip inclinations determine depositional environment? In J.H. Whitmore (editor), *Proceedings of the Ninth International Conference on Creationism*, pp. 588-610. Cedarville, Ohio: Cedarville University International Conference on Creationism.

CAN SANDSTONE CROSS-BED DIP INCLINATIONS DETERMINE DEPOSITIONAL ENVIRONMENT?

John H. Whitmore, Cedarville University, School of Science and Mathematics, 251 N. Main St., Cedarville, Ohio 45314. johnwhitmore@cedarville.edu.

ABSTRACT

Some have recognized that supposed eolian cross-bedded sandstones often lack angle of repose cross-bed inclinations (33-34°) which are common in modern eolian environments. It has previously been reported that sandstones like the Coconino have average cross-bed inclinations of only 20° and lack angle of repose inclinations. Compaction of the dip angles or non-preservation of upper, and steeper, inclinations is often cited to explain this anomaly. Some (incorrectly) claim that subaqueous cross-bed inclinations are less than eolian ones, arguing that relatively low cross-bed angles and averages, like those in the Coconino, demonstrate a subaqueous origin rather than an eolian one.

This study examined and compared over 10,000 cross-bed dip measurements from ancient sandstones (many supposed to be eolian) and modern eolian dunes. Modern dunes do not have the upper part of the dunes eroded away, so it is possible to measure anywhere on the dune. Despite this, it was found that both groups had central tendencies near 20°. The difference in the data sets is best demonstrated by the standard deviations. The middle quartiles of sandstones occurred between 15-24° with a standard deviation of 5.7. The middle quartiles of modern dunes occurred between 9-27°, with a standard deviation of 10.1, nearly double that of ancient sandstones. In other words, modern dune inclinations had a much wider spread than ancient sandstones. Additionally, it was found that modern dunes often have inclination measurements of greater than 30°, which is uncommon in ancient sandstones.

It was found that compaction is not a valid argument for lower-than-expected cross-bed angles, because modern dunes have an abundance of lower angles which are largely absent from the sandstone data sets. This study demonstrates that the spread of cross-bed dip inclinations in sandstones is the important criterion that distinguishes them from eolian deposits and suggests an alternative origin, not the averages of their dips. Additionally, it was found that some sets of sandstone cross-bed inclinations cannot be statistically distinguished from one another irrespective of presumed conventional depositional environment and cross-bed set thickness, specifically in the case of the Grand Canyon's Coconino (eolian), Wescogame (fluvial), and Tapeats (shallow marine) Sandstones.

KEYWORDS

cross-bed dips, cross-bed inclinations, Coconino Sandstone, Tapeats Sandstone, Navajo Sandstone, eolian cross-beds, angle of repose, cross-bed statistics

I. INTRODUCTION AND BACKGROUND

The author has been working on the Coconino Sandstone (Permian, Arizona, USA) for about twenty-five years concluding that the sandstone formed in a subaqueous setting instead of the conventionally accepted desert dune environment (Whitmore and Garner 2018 and citations therein). This conclusion was based on textural, mineralogical, sedimentological, and facies relationship arguments. Maithel (2019) and Maithel et al. (2021) showed that the Coconino does not have the expected eolian-type sedimentology, as is often claimed (Middleton et al. 2003). During our work, we reported that average cross-bed dips in the Coconino were approximately 20° (Emery et al. 2011; Whitmore 2021a, 2021b; Whitmore and Garner 2018), consistent with what others have found in the Coconino for many decades (Maithel 2019; Reiche 1938). This paper is a formal presentation of the work presented in abstract form by Whitmore (2021a, b).

Most geologists realize this average measurement (20°) is far less than the angle of repose for desert dunes, which is about 33-34°. The Coconino often lacks cross-bed dips in the thirties, leading to the erroneous conclusion by some that this conclusively demonstrates a subaqueous origin (Thomas 2021; Thomas and Clarey 2021). Many are unaware that the angle of repose is about the same in air as it is underwater (Allen 1970; Carrigy 1970; Hunter 1985), making steep angles underwater possible. On the other hand, some have erroneously claimed, without consultation of published literature, proper measurements, or data of their own, that the Coconino and other supposed eolian sandstones indeed have relatively steep cross-bed dips near the angle of repose (Hill et al. 2016; Young and Stearley 2008; Strahler 1999). Inconsistently, some authors also want to claim that the cross-beds in "eolian" sandstones like the Coconino and Navajo are "steep" –at the angle of repose yet claiming at the same time the reason authors like myself have not encountered them is that the steeper tops of the eolian dunes have not been preserved (Collins

2022). Recognizing the lack of steep angles in eolian cross-beds, some have suggested the steep angles have been compacted to the lower-than-expected angles (Glennie 1972, p. 1058; Hunter 1981, p. 323; Walker and Harms 1972, p. 280). Most of these claims have been made, incredibly, without making any measurements or citing any data whatsoever, despite cross-bed dip data from numerous sandstones being available at least since 1938 (Reiche). This paper is a collection and presentation of those data so arguments can be made from data instead of assumptions.

As the author was working on the correlation of the Coconino Sandstone across the United States (Whitmore 2019), he began to realize that the Coconino cross-bed dips (Fig. 1) had a different spread of values than dips of modern stabilized dunes, like the Nebraska Sand Hills (Fig. 2). The Nebraska Sand Hills dips were spread between 0-35°, whereas the Coconino dips seemed to cluster around 20°, with very few high or low measurements (Fig. 3). Additionally, McKee and Bigarella had reported "most dips in the Coconino were in the 25-30° range (Fig. 4)," but did not cite data (1979a, p. 199). This was contrary to measurements of the Coconino reported by a contemporary of McKee (Reiche 1938), and later reported by my students (Emery et al. 2011) and Maithel (2019). In reviewing a Tapeats Sandstone paper published by Snelling (2021), the author further realized that other sandstones had a similar distribution of dips to the Coconino. This paper confirms that many other sandstones, regardless of the supposed depositional environment, also have average dips clustered around 20°, and that eolian cross-beds have similar central tendencies—but with different distributions of values.

The goals of this paper is to (1) characterize the cross-bed inclinations of modern eolian dunes from the published literature, (2) characterize the cross-bed inclinations of ancient cross-beds, and (3) compare the sets of data to determine their similarities and differences.

II. METHODS AND DATA COLLECTION

Data were gathered from the literature that contained cross-bed dip data for sandstones and modern eolian deposits (Ahlbrandt and Fryberger 1980; Bigarella 1972; Bigarella and Salamuni 1961; Bigarella et al. 1969; Fryberger et al. 2016; Kiersch 1950; Maithel

Fig. 1. Cross-beds in the Coconino Sandstone at Five-mile Wash near Holbrook, Arizona. The planar bedded set in the middle of the photo is about 0.5 m thick. JHW photo DSC_5430.

Fig. 2. A stabilized sand dune in the Nebraska Sand Hills, about 24 km south of Valentine, Nebraska. Ray Strom and Paul Garner in the photo for scale. JHW photo DSC_1340.

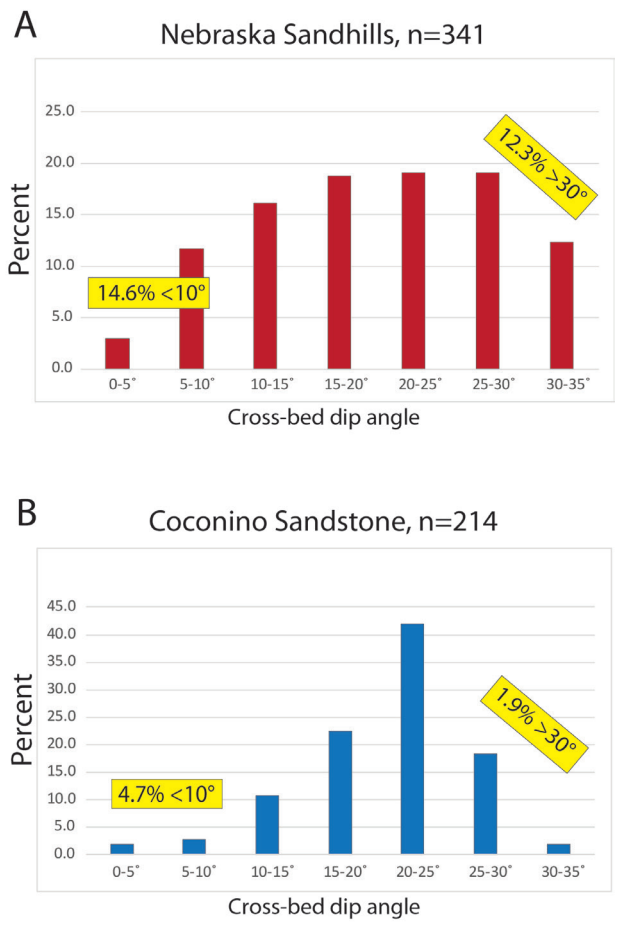

Fig. 3. A comparison between cross-bed dip angles in the Nebraska Sand Hills (A, data from Ahlbrandt and Fryberger 1980) and the Coconino Sandstone from Arizona (B, unpublished data from Whitmore). The sand hills data were plotted in 5-degree bins in Ahlbrandt and Fryberger, so the Coconino was plotted in the same way so a comparison could be made. Note the significant numbers of low and high cross-bed inclinations in the Sand Hills compared to that of the Coconino.

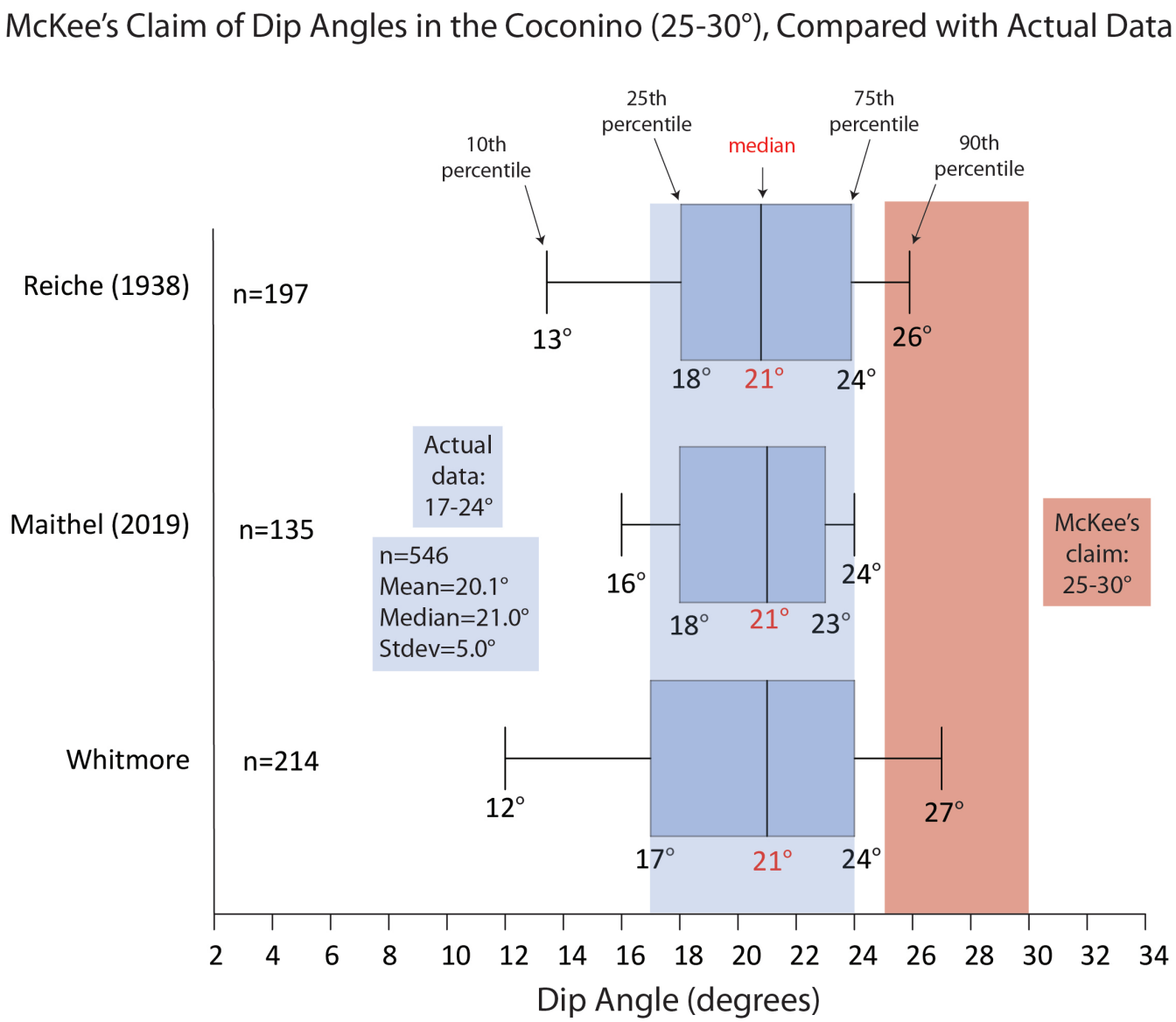

Fig. 4. McKee and Bigarella (1979a, p. 199) claimed that the Coconino had dips "mostly at 25-30°," but when compared to three different sets of data from the Coconino, this conjecture does not hold true. The box plots of the Coconino show the 10th, 25th, 50th, 75th, and 90th percentiles of the data. Most Coconino cross-bed dips fall within the 17-24° range. The data comes from Reiche (1938), Maithel (2019), and unpublished data from Whitmore.

2019; McKee 1940; McKee 1966; McKee 1982; McKee and Bigarella 1979a; McKee and Bigarella 1979b; Reiche 1938; and Whitmore 2019). Sandstone data came primarily from polar plots consisting of 5,242 measurements of 13 sandstones from 88 localities: Botucatú Sandstone of Brazil, Casper Sandstone of Wyoming, Cedar Mesa Sandstone of Utah, Coconino Sandstone of Arizona, De Chelly Sandstone of Arizona, Esplanade Sandstone of Arizona, Manakacha Formation of Arizona, Navajo Sandstone primarily of Utah, Tacuarembó Sandstone of Uruguay, Tapeats Sandstone of Arizona, Tensleep Sandstone primarily of Wyoming, Wescogame Formation of Wyoming, and the Wingate Sandstone of Arizona. None of my data were used in the data set. Modern dunes included measurements from dune fields in Brazil, Uruguay, and New Mexico. The set included 5,785 measurements (855 direct measurements and 4,930 weighted measurements) from 76 dune field localities. Other data from modern dune locations and settings were available, but the data were not always presented in a way that could be used in this study. The author has not measured any cross-bed dips on modern dunes.

The data were presented in many ways, including tables, circular (polar) graphs, and histograms. Some data were interesting, but could not be used, like that from the Nebraska Sand Hills, because it was not presented as individual measurements, but as a collection of measurements in 5-degree bins. It was straightforward to extract the data from tables and histograms, but circular (polar) plots (like Fig. 5) presented somewhat of a challenge. It was difficult to read the points from these graphs consistently and accurately. WebPlotDigitizer was used to aid in the collection of these kinds of data. The online application allowed an origin and two points to be plotted on the graph (directly on the computer screen) to let the application know the dimensions of the graph. Points could then be plotted on the graph by using a mouse and marking colored dots, to be sure all the points

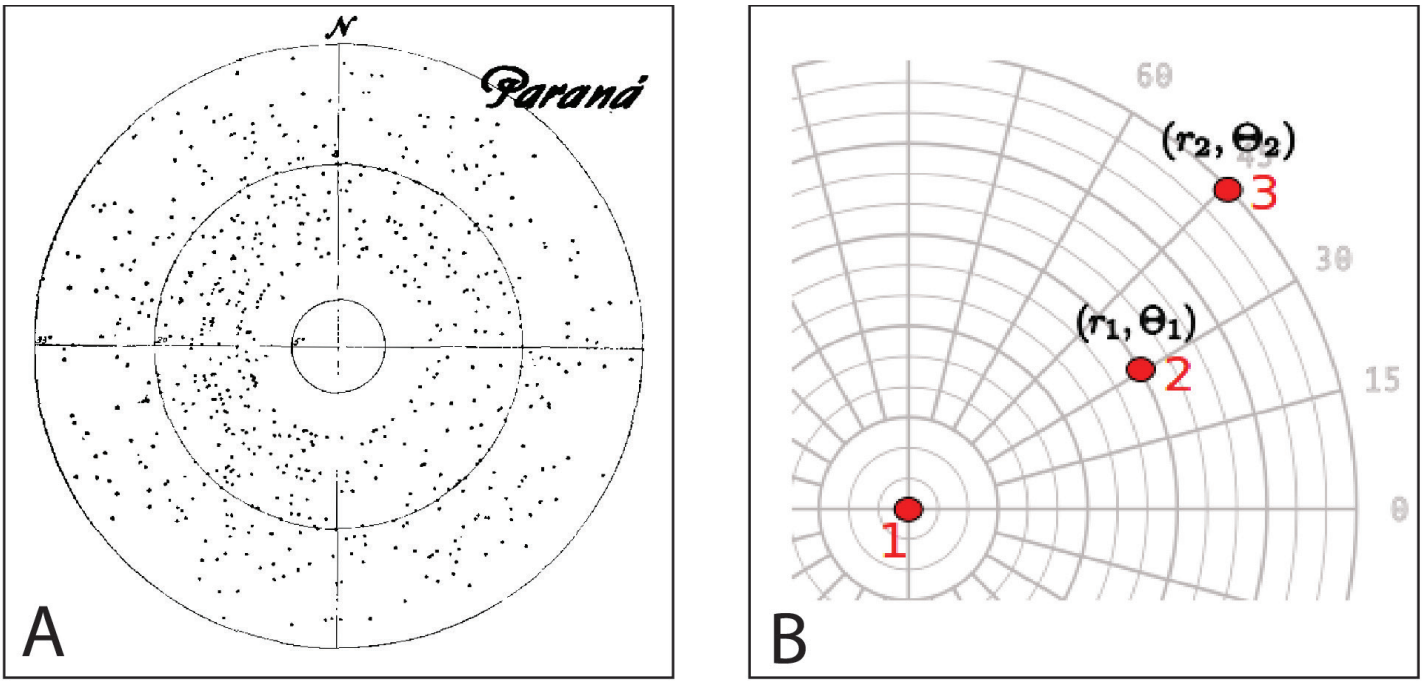

Fig. 5. A. An example of a polar data plot from Bigarella and Salamuni (1961, p. 1094). The circles represent 5, 20, and 35° dips. B. To use polar plot data, WebPlotDigitizer was used to get an accurate azimuth and dip angle. This web application allows superposition and calibration of a plot like "A" in the software. Points can be clicked on and then tabulated in a spreadsheet as they are selected.

are accounted for, the values of which are saved. Poor resolution and overlapping points on some of the plots led to slight differences in the number of points I measured and those reported by the authors.

A large amount of eolian data were presented in table form as a number of values (n) and a mean ($\bar{x}$). In these cases, a weighted mean was calculated for the data. An example set of data are shown in Table 1. The numbers of measurements (n) for Ipanema are 56, 39, and 23, with respective average dips of 12.4, 12.1, and 10.0 degrees, for a total of 118 measurements. The calculation for a weighted mean would be the following:

$$\bar{x} = \frac{\sum w_i x_i}{\Sigma_{w_i}}$$

(where w_i = the number of measurements and x_i = average dip of the measurements). Substituting the actual values in we get a weighted mean of 11.8°:

$$\frac{(56\times12.4°)+(39\times12.1°)+(23\times10.0°)}{118} = \frac{1396}{118} = 11.8^{\circ}$$

A calculation like this was done for 4,930 of the dune measurements. These data were useful for calculating means of dunes, but not as useful as individual dune measurements, which showed the spread of the data. Microsoft Excel and Golden Software's Grapher were used to analyze and graph the data.

III. RESULTS

Table 2 is a summary of the measurements from both modern and ancient cross-bedded deposits using the collection methods described above. Table 3 shows a summary of the overall results.

A. Sandstones and eolian dunes have similar central tendencies of cross-bed inclinations

Analysis of the data showed that dip inclinations in modern dunes have similar central tendencies to those found in ancient sandstones (Fig. 6, Table 3). Since the data were collected and calculated in two different ways for modern dunes, two plots are shown in Fig. 6, and two rows of results are shown in Table 3, comparing the two methods. Table 3 summarizes the means and medians of cross-bed inclinations for the weighted means of dunes (19.8°, 19.8°), actual measurements of dunes (17.8°, 15.0°) and sandstones (19.8°, 19.9°). Note that the central tendencies of all these measurements are within a few degrees of each other, independent of whether the deposit is modern or ancient. The "dunes" category in Fig. 6 is most similar to the measurement method used for "sandstones."

B. Sandstones and eolian dunes have different standard deviations for their dip distributions

Fig. 7 shows a comparison of the dip angles of 855 modern eolian dunes with 5,242 sandstone foresets. The data were converted into percentages so the two sets of data could be compared. The plot shows eolian dunes have a much wider "spread" than the sandstone data. This can be expressed as standard deviation (10.1 for eolian dunes and 5.7 for sandstones) and visualized as quartiles (the lower part of Fig. 7). Eolian dunes have nearly twice the standard deviation as sandstones which is expressed by the wider spread of the data when compared to the sandstones. The plot of eolian dunes is bimodal, peaking at about 10 and 33 degrees; the sandstone plot is unimodal, peaking at about 20 degrees. The plots show these are two different sets of data.

Table 1. An example of how some of the cross-bed dip data was published (Table 1 from Bigarella 1972, p. 26). In this example a number of measurements are reported along with a maximum and average dip. In these cases, a weighted mean was calculated (explained in text).

Locality		Number of Measurements	Average dip direction	Maximum dip	Average dip	Consistency ratio
Ipanema (Paraná)	A	56	N76°E	34°	12.4°	0.56
	B	39	S71°W	33°	12.1°	0.44
	C	23	S82°E	19°	10.0°	0.50
General		118	E	34°	11.8°	0.22
Barra do Sul (Sta. Catarina)	1	49	N4°2E	31°	15.0°	0.13
	2	44	N01°E	29°	13.4°	0.24
General		93	N16°E	31°	14.3°	0.17

Table 2. References and data of foreset dip angles of rock and modern eolian deposits used for this paper. "Reported" is data directly reported in a paper; "measured" means Whitmore measured or made calculations from the information in the report; "nr" means not reported by author; and "—" means not applicable for the particular reference.

Reference	Substance	Formation	Age	Location	Type of data	n measured	n reported	mean measured	mean reported	median measured	median reported	max measured	max reported	min measured	min reported	sd measured	sd reported
Bigarella and Salamuni 1961 (p. 1094)	rock	Botucatú Sandstone	Jurassic-Cretaceous	Minas Gerais, Brazil	Polar plot	220	220	18.8	19.6	18.9	nr	33.6	33	1.9	nr	6.9	nr
Bigarella and Salamuni 1961 (p. 1094)	rock	Botucatú Sandstone	Jurassic-Cretaceous	Paraná, Brazil	Polar plot	626	646	19.5	19.5	19.1	nr	33.3	33	7.9	nr	6.2	nr
Bigarella and Salamuni 1961 (p. 1094)	rock	Botucatú Sandstone	Jurassic-Cretaceous	Rio Grande Do Sul, Brazil	Polar plot	598	615	20.5	20.8	20.2	nr	32.5	33	9.5	nr	6.2	nr
Bigarella and Salamuni 1961 (p. 1094)	rock	Botucatú Sandstone	Jurassic-Cretaceous	São Paulo, Brazil	Polar plot	650	676	20.1	20.3	20	nr	32.5	33	9.7	nr	6.2	nr
Bigarella and Salamuni 1961 (p. 1094)	rock	Botucatú Sandstone	Jurassic-Cretaceous	Santa Catarina, Brazil	Polar plot	386	391	19.9	19.5	20.1	nr	32.9	33	8.1	nr	6	nr
Bigarella and Salamuni 1961 (p. 1094)	rock	Tacuarembó Sandstone	Jurassic-Cretaceous	Uruguay	Polar plot	351	344	21.1	21.2	21.9	nr	33.3	33	3.8	nr	6.4	nr
Kiersch-1950 (p. 932)	rock	Navajo Sandstone, upper unit	Triassic	Utah, South Saleratus Creek	Polar plot	43	nr	17.2	nr	18.8	nr	24.9	nr	4.6	nr	4.8	nr
Kiersch-1950 (p. 932)	rock	Navajo Sandstone, upper unit	Triassic	Utah, Upper Buckhorn Wash	Polar plot	44	nr	16.4	nr	16.6	nr	31.2	nr	4.6	nr	6.6	nr
Kiersch-1950 (p. 932)	rock	Navajo Sandstone, upper unit	Triassic	Utah, San Rafael River	Polar plot	34	nr	18	nr	19.7	nr	24.5	nr	6.8	nr	4.6	nr
Kiersch-1950 (p. 933)	rock	Navajo Sandstone, middle unit	Triassic	Utah, Upper Buckhorn Wash	Polar plot	35	nr	16.1	nr	16.2	nr	25.1	nr	5.1	nr	5.2	nr

Table 2, continued

Kiersch-1950 (p. 933)	rock	Navajo Sandstone, middle unit	Triassic	Utah, Central Buckhorn Wash	Polar plot	36	nr	18.2	nr	19.1	nr	26.4	nr	4.3	nr	5.4	nr
Kiersch-1950 (p. 933)	rock	Navajo Sandstone, middle unit	Triassic	Utah, San Rafael River	Polar plot	37	nr	17.4	nr	18.2	nr	23.6	nr	7.4	nr	4.1	nr
Reiche 1938 (p. 928)	rock	Cedar Mesa	Permian	Utah, 15 mi NE Mexican Hat	Polar plot	67	67	18.7	nr	18.5	nr	33	nr	2.5	nr	5.7	nr
Reiche 1938 (p. 908)	rock	Coconino Sandstone	Permian	Arizona, Aubrey Cliffs	Polar plot	38	38	19.1	nr	19.2	nr	24.2	nr	10.5	nr	2.9	nr
Reiche 1938 (p. 908)	rock	Coconino Sandstone	Permian	Arizona, Bunker Trail	Polar plot	53	52	21.2	nr	21.4	nr	30	nr	6.6	nr	4.5	nr
Reiche 1938 (p. 908)	rock	Coconino Sandstone	Permian	Arizona, Clear Creek (lower?)	Polar plot	59	55	22.5	nr	22.8	nr	33.8	nr	10.8	nr	4.2	nr
Reiche 1938 (p. 925)	rock	Coconino Sandstone	Permian	Arizona, east of Holbrook	Polar plot	47	47	17.6	nr	19.2	nr	26.7	nr	6.9	nr	5.2	nr
Reiche 1938 (p. 925)	rock	DeChelly Sandstone	Permian	Arizona, Canyon DeChelly	Polar plot	30	30	23.1	nr	23.8	nr	33.4	nr	13.6	nr	4.3	nr
Reiche 1938 (p. 925)	rock	DeChelly Sandstone	Permian	Arizona, Monument Valley	Polar plot	52	52	20.1	nr	21	nr	28.4	nr	7.7	nr	5.1	nr
Reiche 1938 (p. 928)	rock	Navajo Sandstone	Triassic	Arizona, Kayenta	Polar plot	33	32	22.1	nr	23.1	nr	36.2	nr	10.9	nr	5.4	nr
Reiche 1938 (p. 928)	rock	Wingate Sandstone	Triassic	New Mexico, Fort Wingate	Polar plot	48	48	18.8	nr	20.2	nr	30	nr	8.6	nr	5.6	nr
McKee 1940 (p. 813)	rock	Tapeats Sandstone	Cambrian	Arizona, Cremation	Polar plot	34	nr	21.2	nr	21.1	nr	27.6	nr	14	nr	3.4	nr
McKee 1940 (p. 813)	rock	Tapeats Sandstone	Cambrian	Arizona, West Yaki Trail	Polar plot	29	nr	20.2	nr	20.9	nr	26.9	nr	11.7	nr	4.3	nr
McKee 1940 (p. 813)	rock	Tapeats Sandstone	Cambrian	Arizona, Pipe Creek east	Polar plot	30	nr	19.9	nr	20.8	nr	27.1	nr	9.1	nr	4.7	nr
McKee 1940 (p. 813)	rock	Tapeats Sandstone	Cambrian	Arizona, Bright Angel Trail	Polar plot	31	nr	19	nr	19.4	nr	27.7	nr	8.4	nr	5.7	nr
McKee 1940 (p. 813)	rock	Tapeats Sandstone	Cambrian	Arizona, Hermit Trail	Polar plot	29	nr	21.4	nr	22.8	nr	27.6	nr	11.4	nr	4.8	nr
McKee 1940 (p. 813)	rock	Tapeats Sandstone	Cambrian	Arizona, Quartermaster	Polar plot	30	nr	20.1	nr	20.5	nr	27.9	nr	11.6	nr	5.4	nr

Table 2, continued

McKee 1982 (p. 218 A)	rock	Manakacha Formation	Pennsylvanian	Arizona, Bunker Trail	Polar plot	21	nr	19.4	nr	19.7	nr	27.8	nr	12.3	nr	4.1	nr
McKee 1982 (p. 218 B)	rock	Manakacha Formation	Pennsylvanian	Arizona, Kaibab Trail south	Polar plot	26	nr	19.6	nr	19.2	nr	26.5	nr	12.1	nr	4	nr
McKee 1982 (p. 218 C)	rock	Manakacha Formation	Pennsylvanian	Arizona, Hermit Trail	Polar plot	24	nr	20.1	nr	20.1	nr	28.1	nr	11.6	nr	4.5	nr
McKee 1982 (p. 218 D)	rock	Manakacha Formation	Pennsylvanian	Arizona, Kaibab Trail north	Polar plot	26	nr	23.2	nr	24	nr	31.4	nr	15.8	nr	4.8	nr
McKee 1982 (p. 218 E)	rock	Manakacha Formation	Pennsylvanian	Arizona, Fishtail Canyon	Polar plot	21	nr	19	nr	19	nr	27.3	nr	11.8	nr	3.6	nr
McKee 1982 (p. 218 F)	rock	Manakacha Formation	Pennsylvanian	Arizona, Hermit Trail	Polar plot	28	nr	19.3	nr	18.3	nr	28.8	nr	11.2	nr	4.9	nr
McKee 1982 (p. 218 G)	rock	Manakacha Formation	Pennsylvanian	Arizona, Havasu Canyon	Polar plot	24	nr	19.2	nr	20.1	nr	24.9	nr	11.9	nr	3.9	nr
McKee 1982 (p. 218 H)	rock	Manakacha Formation	Pennsylvanian	Arizona, Toroweap Valley	Polar plot	26	nr	20.2	nr	20.5	nr	28	nr	12.7	nr	3.8	nr
McKee 1982 (p. 218 I)	rock	Manakacha Formation	Pennsylvanian	Arizona, Whitmore Wash	Polar plot	26	nr	17.4	nr	18	nr	21.7	nr	11.5	nr	2.9	nr
McKee 1982 (p. 219 J)	rock	Manakacha Formation	Pennsylvanian	Arizona, Grand Wash Cliffs	Polar plot	14	nr	17.3	nr	17	nr	26	nr	12	nr	4	nr
McKee 1982 (p. 219 K)	rock	Manakacha Formation	Pennsylvanian	Arizona, Hidden Canyon	Polar plot	14	nr	18.1	nr	18	nr	26	nr	10.3	nr	4.3	nr
McKee 1982 (p. 230 A)	rock	Wescogame Formation	Pennsylvanian	Arizona, House Rock Canyon	Polar plot	29	nr	17.9	nr	17.6	nr	25.6	nr	10.3	nr	3.6	nr
McKee 1982 (p. 230 B)	rock	Wescogame Formation	Pennsylvanian	Arizona, Marble Canyon	Polar plot	20	nr	20.8	nr	21.1	nr	26.5	nr	14.6	nr	3.7	nr
McKee 1982 (p. 230 C)	rock	Wescogame Formation	Pennsylvanian	Arizona, Horsetrail Canyon	Polar plot	24	nr	20.8	nr	21.1	nr	27.4	nr	13.7	nr	3.6	nr
McKee 1982 (p. 230 D)	rock	Wescogame Formation	Pennsylvanian	Arizona, Bunker Trail	Polar plot	24	nr	19.4	nr	19.6	nr	27.4	nr	11	nr	4.9	nr
McKee 1982 (p. 230 E)	rock	Wescogame Formation	Pennsylvanian	Arizona, Grandview Trail	Polar plot	23	nr	21.2	nr	21.9	nr	26.6	nr	11.8	nr	3.8	nr
McKee 1982 (p. 230 F)	rock	Wescogame Formation	Pennsylvanian	Arizona, Grandview Trail	Polar plot	22	nr	19.3	nr	20.4	nr	27	nr	9.8	nr	5	nr

Table 2, continued

McKee 1982 (p. 230 G)	rock	Wescogame Formation	Pennsylvanian	Arizona, Kaibab Trail south	Polar plot	26	nr	19.6	nr	19.6	nr	26.7	nr	11.7	nr	4.5	nr
McKee 1982 (p. 230 H)	rock	Wescogame Formation	Pennsylvanian	Arizona, Bright Angel Trail	Polar plot	22	nr	20.6	nr	21.8	nr	27.1	nr	13	nr	3.8	nr
McKee 1982 (p. 230 I)	rock	Wescogame Formation	Pennsylvanian	Arizona, Hermit Trail	Polar plot	29	nr	20.1	nr	19.8	nr	30.3	nr	11.4	nr	5.6	nr
McKee 1982 (p. 231 J)	rock	Wescogame Formation	Pennsylvanian	Arizona, Bass Trail	Polar plot	27	nr	21.2	nr	21	nr	27.8	nr	13.2	nr	4.1	nr
McKee 1982 (p. 231 K)	rock	Wescogame Formation	Pennsylvanian	Arizona, Topocoba Trail	Polar plot	28	nr	20.9	nr	21.8	nr	26.9	nr	11.7	nr	3.8	nr
McKee 1982 (p. 231 L)	rock	Wescogame Formation	Pennsylvanian	Arizona, Havasu Canyon	Polar plot	28	nr	18.7	nr	18.4	nr	28	nr	9.7	nr	4.9	nr
McKee 1982 (p. 232 A)	rock	Wescogame Formation	Pennsylvanian	Arizona, Kaibab Trial north	Polar plot	28	nr	19.9	nr	19.8	nr	27.7	nr	11.9	nr	4.4	nr
McKee 1982 (p. 232 B)	rock	Wescogame Formation	Pennsylvanian	Arizona, Fishtail Canyon	Polar plot	20	nr	20.1	nr	21	nr	25.4	nr	11.6	nr	3.5	nr
McKee 1982 (p. 232 C)	rock	Wescogame Formation	Pennsylvanian	Tuckup Canyon	Polar plot	30	nr	20.2	nr	19.7	nr	29.2	nr	11.5	nr	4.1	nr
McKee 1982 (p. 232 D)	rock	Wescogame Formation	Pennsylvanian	Arizona, Toroweap Valley	Polar plot	26	nr	20.5	nr	21	nr	28	nr	15	nr	3.3	nr
McKee 1982 (p. 232 E)	rock	Wescogame Formation	Pennsylvanian	Arizona, Toroweap Valley	Polar plot	19	nr	19.9	nr	21.2	nr	26.4	nr	11.9	nr	3.7	nr
McKee 1982 (p. 232 F)	rock	Wescogame Formation	Pennsylvanian	Arizona, Whitmore Wash	Polar plot	26	nr	21.6	nr	20.7	nr	28.2	nr	13.7	nr	4.2	nr
McKee 1982 (p. 232 G)	rock	Wescogame Formation	Pennsylvanian	Arizona, Separation Canyon	Polar plot	28	nr	17.6	nr	17.7	nr	23.9	nr	10.4	nr	3.8	nr
McKee 1982 (p. 232 H)	rock	Wescogame Formation	Pennsylvanian	Arizona, Guano Cave lower	Polar plot	30	nr	20.1	nr	19.9	nr	27.9	nr	10.8	nr	4.6	nr
McKee 1982 (p. 232 I)	rock	Wescogame Formation	Pennsylvanian	Arizona, Guano Cave upper	Polar plot	29	nr	19.8	nr	20.7	nr	28	nr	11.7	nr	4.9	nr
McKee 1982 (p. 233 J)	rock	Wescogame Formation	Pennsylvanian	Arizona, Parashant Canyon	Polar plot	27	nr	20.3	nr	20.9	nr	29.2	nr	12.4	nr	4.5	nr
McKee 1982 (p. 233 K)	rock	Wescogame Formation	Pennsylvanian	Arizona, Snap Canyon	Polar plot	30	nr	17.9	nr	17.6	nr	28.6	nr	9.5	nr	5.1	nr

Table 2, continued

McKee 1982 (p. 233 L)	rock	Wescogame Formation	Pennsylvanian	Arizona, Pigeon Wash	Polar plot	24	nr	18.9	nr	19.7	nr	26.5	nr	8.5	nr	4.6	nr
McKee 1982 (p. 238 A)	rock	Esplanade Sandstone	Permian	Arizona, Twentynine Mile Canyon	Polar plot	28	nr	17.5	nr	17.7	nr	23.5	nr	7.9	nr	4	nr
McKee 1982 (p. 238 B)	rock	Esplanade Sandstone	Permian	Arizona, Bunker Trail	Polar plot	33	nr	21.4	nr	22.4	nr	26.6	nr	12.8	nr	3.2	nr
McKee 1982 (p. 238 C)	rock	Esplanade Sandstone	Permian	Arizona, Bunker Trail	Polar plot	22	nr	23.3	nr	23.4	nr	32.7	nr	12	nr	4.8	nr
McKee 1982 (p. 238 D)	rock	Esplanade Sandstone	Permian	Arizona, Kaibab Trail south	Polar plot	29	nr	17.2	nr	18.7	nr	26.2	nr	3.4	nr	5.7	nr
McKee 1982 (p. 238 E)	rock	Esplanade Sandstone	Permian	Arizona, Bright Angel Trail	Polar plot	29	nr	16.6	nr	16.2	nr	26.5	nr	6.3	nr	5.6	nr
McKee 1982 (p. 238 F)	rock	Esplanade Sandstone	Permian	Arizona, Hermit Trail	Polar plot	29	nr	19.8	nr	19.8	nr	27.9	nr	11.6	nr	4.4	nr
McKee 1982 (p. 238 G)	rock	Esplanade Sandstone	Permian	Arizona, Kaibab Trail north	Polar plot	26	nr	19.8	nr	21	nr	27.7	nr	6.9	nr	5.9	nr
McKee 1982 (p. 238 H)	rock	Esplanade Sandstone	Permian	Arizona, Shinumo Trail	Polar plot	22	nr	18.8	nr	18.9	nr	24.7	nr	11.3	nr	3.6	nr
McKee 1982 (p. 238 I)	rock	Esplanade Sandstone	Permian	Arizona, Bass Trail	Polar plot	29	nr	19.2	nr	19.6	nr	26.9	nr	10	nr	4.4	nr
McKee 1982 (p. 239 J)	rock	Esplanade Sandstone	Permian	Arizona, Fishtail Canyon	Polar plot	25	nr	19.3	nr	19	nr	23.7	nr	13.7	nr	2.9	nr
McKee 1982 (p. 239 K)	rock	Esplanade Sandstone	Permian	Arizona, Havasu Canyon	Polar plot	31	nr	18.8	nr	19.3	nr	27.4	nr	10	nr	5.2	nr
McKee 1982 (p. 239 L)	rock	Esplanade Sandstone	Permian	Arizona, Tuckup Canyon	Polar plot	31	nr	16.9	nr	16.4	nr	23.3	nr	10.9	nr	3.6	nr
McKee 1982 (p. 240 A)	rock	Esplanade Sandstone	Permian	Arizona, Toroweap Valley	Polar plot	29	nr	17.6	nr	17.3	nr	26	nr	8.5	nr	3.9	nr
McKee 1982 (p. 240 B)	rock	Esplanade Sandstone	Permian	Arizona, Prospect Valley	Polar plot	30	nr	20.6	nr	20.6	nr	27.6	nr	15.7	nr	3.5	nr
McKee 1982 (p. 240 C)	rock	Esplanade Sandstone	Permian	Arizona, Whitmore Wash	Polar plot	30	nr	18.8	nr	18.8	nr	27.8	nr	7.8	nr	4.6	nr
McKee 1982 (p. 240 D)	rock	Esplanade Sandstone	Permian	Arizona, Snap Canyon	Polar plot	30	nr	19.5	nr	20.3	nr	27.7	nr	9.3	nr	4.9	nr

Table 2, continued

McKee 1982 (p. 240 E)	rock	Esplanade Sandstone	Permian	Arizona, Pigeon Wash	Polar plot	30	nr	18.6	nr	17.6	nr	27.3	nr	9.3	nr	5.3	nr
McKee 1982 (p. 240 F)	rock	Esplanade Sandstone	Permian	Arizona, Hidden Canyon	Polar plot	22	nr	19.9	nr	20.1	nr	26.3	nr	13.7	nr	3	nr
McKee 1982 (p. 240 G)	rock	Pakoon Limestone	Permian	Arizona, Snap Canyon	Polar plot	30	nr	16	nr	16.5	nr	21.6	nr	9.6	nr	3.2	nr
McKee 1982 (p. 240 H)	rock	Pakoon Limestone	Permian	Arizona, Grand Gulch	Polar plot	31	nr	20	nr	20.5	nr	26.5	nr	11.3	nr	4.1	nr
McKee 1982 (p. 240 I)	rock	Pakoon Limestone	Permian	Arizona, south Hidden Canyon	Polar plot	19	nr	16.4	nr	16.4	nr	21.9	nr	11.4	nr	2.9	nr
Maithel 2019 (p. 175-176)	rock	Coconino Sandstone	Permian	Arizona (various)	Data table	—	135	—	19.8	21	nr	—	27	—	7	4	nr
Fryberger et al 2016	rock	Casper Sandstone	Permian	Wyoming	Measured section	—	18	20.1	nr	22	nr	—	27	—	9	4.5	nr
Fryberger et al 2016	rock	Tensleep Sandstone flat-top	Permian	Wyoming	Measured section	—	28	22.2	nr	23	nr	—	34	—	11	5.5	nr
Fryberger et al 2016	rock	Tensleep Sandstone Rock Canyon	Permian	Wyoming	Measured section	—	6	21.2	nr	21	nr	—	26	—	17	3.3	nr
Fryberger et al 2016	rock	Tensleep Sandstone Paradise Valley	Permian	Wyoming	Measured section	—	13	18.9	nr	19	nr	—	24	—	11	3.9	nr
Bigarella et al 1969,I Table III, Fig 9	eolian	coastal dune	modern	Praia de Leste, Brazil	Figures, Table 3	—	52	—	21.6	24	nr	—	38	5	nr	9.4	nr
Bigarella et al 1969,II Table III, Fig 9	eolian	coastal dune	modern	Praia de Leste, Brazil	Figures, Table 3	—	23	—	20.7	17	nr	—	39	5	nr	12.7	nr
Bigarella et al 1969,III Table III, Fig 9	eolian	coastal dune	modern	Praia de Leste, Brazil	Figures, Table 3	—	32	—	18.6	—	nr	—	34	—	nr	—	nr
Bigarella et al 1969,IV Table III, Fig 9	eolian	coastal dune	modern	Praia de Leste, Brazil	Figures, Table 3	—	67	—	17.2	15	nr	—	39	5	nr	7.9	nr
Bigarella et al 1969,V Table III, Fig 9	eolian	coastal dune	modern	Praia de Leste, Brazil	Figures, Table 3	—	27	—	25	28.5	nr	—	38	6	nr	9.7	nr
Bigarella et al 1969,VI Table III, Fig 9	eolian	coastal dune	modern	Praia de Leste, Brazil	Figures, Table 3	—	11	—	15.5	14	nr	—	26	11	nr	4.2	nr
Bigarella et al 1969,VII Table III, Fig 9	eolian	coastal dune	modern	Praia de Leste, Brazil	Figures, Table 3	—	21	—	13.4	13	nr	—	22	6	nr	4.9	nr

Table 2, continued

Bigarella et al 1969, A Table IV, Fig. 10 p. 31-34	eolian	coastal dune	modern	Porto Novo	Figures, Table IV	—	121	—	20.7	18.5	nr	—	42	4	nr	11	nr
Bigarella et al 1969, A' Table IV, Fig. 10 p. 31-34	eolian	coastal dune	modern	Porto Novo	Figures, Table IV	—	64	—	22.7	—	nr	—	40	—	nr	—	nr
Bigarella et al 1969, A" Table IV, Fig. 10 p. 31-34	eolian	coastal dune	modern	Porto Novo	Figures, Table IV	—	57	—	18.5	—	nr	—	42	—	nr	—	nr
Bigarella et al 1969, B Table IV, Fig. 10 p. 31-34	eolian	coastal dune	modern	Porto Novo	Figures, Table IV	—	40	—	25.8	30.5	nr	—	40	2	nr	12.7	nr
Bigarella et al 1969, C Table IV, Fig. 10 p. 31-34	eolian	coastal dune	modern	Guaramar	Figures, Table IV	—	18	—	8.9	8	nr	—	20	3	nr	4	nr
Bigarella et al 1969, D Table IV, Fig. 10 p. 31-34	eolian	coastal dune	modern	Guaramar	Figures, Table IV	—	16	—	13.8	12	nr	—	29	7	nr	5.9	nr
Bigarella et al 1969, E Table IV, Fig. 10 p. 31-34	eolian	coastal dune	modern	Guaramar	Figures, Table IV	—	6	—	12.8	13.5	nr	—	20	7	nr	4.4	nr
Bigarella et al 1969, F Table IV, Fig. 10 p. 31-34	eolian	coastal dune	modern	Guaramar	Figures, Table IV	—	17	—	19.4	13.5	nr	—	35	2	nr	11.2	nr
McKee and Bigarella 1979 (p. 120; from Bigarella 1975)	eolian	coastal dunes, parabolic	modern	Lagoa dune field, Brazil	Table 11	—	366	—	19.6	—	nr	—	37	—	nr	—	nr
McKee and Bigarella 1979 (p. 121; from Bigarella 1975)	eolian	coastal dunes, parabolic	modern	Lagoa dune field, Brazil	Table 12	—	25	14.1	nr	13	nr	28	nr	3	nr	6.5	nr
McKee and Bigarella 1979 (p. 122; from Bigarella 1975)	eolian	coastal dunes, parabolic	modern	Lagoa dune field, Brazil	Table 13	—	54	22.3	nr	22	nr	37	nr	3	nr	8.2	nr
McKee 1966 (p. 19-21)	eolian	gypsum sand	modern	White Sands, New Mexico	Figure 6	64	64	18.6	nr	19	nr	33	33	5	5	9.9	nr
McKee 1966 (p. 22-24)	eolian	gypsum sand	modern	White Sands, New Mexico	Figure 7	78	78	18.8	nr	17	nr	35	35	5	5	10.3	nr
McKee 1966 (p. 41-43)	eolian	gypsum sand	modern	White Sands, New Mexico	Figure 8	69	69	19	nr	18	nr	34	34	5	5	8.6	nr
McKee 1966 (p. 44-46)	eolian parabolic	gypsum sand	modern	White Sands, New Mexico	Figure 9	26	26	18.3	nr	20	nr	34	34	5	5	8.9	nr
Bigarella 1972 (p. 28, Figure 11-IA)	eolian	beach dune	modern	Guairamar, Praia de Leste Parana, Brazil	Polar plot	36	nr	10.5	nr	8.3	nr	32.4	nr	0.3	nr	6.2	nr
Bigarella 1972 (p. 28, Figure 11-IB)	eolian	beach dune	modern	Guairamar, Praia de Leste Parana, Brazil	Polar plot	39	nr	12.5	nr	10	nr	30	nr	3.9	nr	6.7	nr

Table 2, continued

Bigarella 1972 (p. 28, Figure 11-IC)	eolian	beach dune	modern	Guairamar, Praia de Leste Parana, Brazil	Polar plot	69	nr	9.2	nr	8.3	nr	24	nr	1.3	nr	4.6	nr
Bigarella 1972 (p. 45, Table 3A)	eolian	gypsum sand	modern	White Sands, New Mexico	Table	—	58	—	21.3	—	nr	—	36	—	nr	—	nr
Bigarella 1972 (p. 45, Table 3B)	eolian	gypsum sand	modern	White Sands, New Mexico	Table	—	52	—	21.2	—	nr	—	34	—	nr	—	nr
Bigarella 1972 (p. 45, Table 3C)	eolian	gypsum sand	modern	White Sands, New Mexico	Table	—	73	—	18.2	—	nr	—	39	—	nr	—	nr
Bigarella 1972 (p. 45, Table 3D)	eolian	gypsum sand	modern	White Sands, New Mexico	Table	—	161	—	14.6	—	nr	—	32	—	nr	—	nr
Bigarella 1972 (p. 50, Table 4)	eolian	coastal dunes	modern	Para Salinopolis	Table	—	60	—	22	—	nr	—	38	—	nr	—	nr
Bigarella 1972 (p. 50, Table 4)	eolian	coastal dunes	modern	Piaui Luiz Correia	Table	—	145	—	21.2	—	nr	—	38	—	nr	—	nr
Bigarella 1972 (p. 50, Table 4)	eolian	coastal dunes	modern	Ceara Paracuru	Table	—	109	—	26.1	—	nr	—	40	—	nr	—	nr
Bigarella 1972 (p. 50, Table 4)	eolian	coastal dunes	modern	Cera Fortaleza	Table	—	47	—	20	—	nr	—	34	—	nr	—	nr
Bigarella 1972 (p. 50, Table 4)	eolian	coastal dunes	modern	Cera Majorlandia	Table	—	67	—	18.8	—	nr	—	34	—	nr	—	nr
Bigarella 1972 (p. 50, Table 4)	eolian	coastal dunes	modern	RGN Tibau	Table	—	48	—	20.5	—	nr	—	32	—	nr	—	nr
Bigarella 1972 (p. 50, Table 4)	eolian	coastal dunes	modern	RGN Sao Bento do Norte	Table	—	70	—	18.3	—	nr	—	34	—	nr	—	nr
Bigarella 1972 (p. 50, Table 4)	eolian	coastal dunes	modern	RGN Touros	Table	—	37	—	19.7	—	nr	—	37	—	nr	—	nr
Bigarella 1972 (p. 50, Table 4)	eolian	coastal dunes	modern	RGN Genipabu	Table	—	41	—	14.8	—	nr	—	28	—	nr	—	nr
Bigarella 1972 (p. 50, Table 4)	eolian	coastal dunes	modern	RGN Natal	Table	—	83	—	20	—	nr	—	36	—	nr	—	nr
Bigarella 1972 (p. 50, Table 4)	eolian	coastal dunes	modern	Fernando de Noronha	Table	—	35	—	20.6	—	nr	—	20.6	—	nr	—	nr
Bigarella 1972 (p. 50, Table 4)	eolian	coastal dunes	modern	Fsergipe Aracaju	Table	—	69	—	26.1	—	nr	—	26.1	—	nr	—	nr

Table 2, continued

Bigarella 1972 (p. 50, Table 4)	eolian	coastal dunes	modern	RDJ Cabo Frio a	Table	—	107	—	21.1	—	nr	—	21.1	—	nr	—	nr
Bigarella 1972 (p. 50, Table 4)	eolian	coastal dunes	modern	RDJ Cabo Frio b	Table	—	83	—	22.7	—	nr	—	22.7	—	nr	—	nr
Bigarella 1972 (p. 50, Table 4)	eolian	coastal dunes	modern	Parana Jardim Sao Pedro	Table	—	233	—	19.2	—	nr	—	19.2	—	nr	—	nr
Bigarella 1972 (p. 50, Table 4)	eolian	coastal dunes	modern	Parana Guairamar Porto Novo	Table	—	218	—	19.8	—	nr	—	19.8	—	nr	—	nr
Bigarella 1972 (p. 53, Table 5)	eolian	coastal dunes	modern	Barra do Sul	Table	—	78	—	12.3	—	nr	—	32	—	nr	—	nr
Bigarella 1972 (p. 53, Table 5)	eolian	coastal dunes	modern	Praia dos Ingleses	Table	—	78	—	17	—	nr	—	35	—	nr	—	nr
Bigarella 1972 (p. 53, Table 5)	eolian	coastal dunes	modern	Praia do Santinho	Table	—	44	—	20.2	—	nr	—	34	—	nr	—	nr
Bigarella 1972 (p. 53, Table 5)	eolian	coastal dunes	modern	Lagoa	Table	—	158	—	17.7	—	nr	—	32	—	nr	—	nr
Bigarella 1972 (p. 53, Table 5)	eolian	coastal dunes	modern	Praia do Pantano do Sul	Table	—	75	—	14.6	—	nr	—	30	—	nr	—	nr
Bigarella 1972 (p. 53, Table 5)	eolian	coastal dunes	modern	Pinheira	Table	—	70	—	18.7	—	nr	—	33	—	nr	—	nr
Bigarella 1972 (p. 53, Table 5)	eolian	coastal dunes	modern	Zareia garopaba	Table	—	96	—	22.1	—	nr	—	36	—	nr	—	nr
Bigarella 1972 (p. 53, Table 5)	eolian	coastal dunes	modern	Praia N da Ponta da Careca do Velho	Table	—	125	—	24.2	—	nr	—	37	—	nr	—	nr
Bigarella 1972 (p. 53, Table 5)	eolian	coastal dunes	modern	5 km south of Henrique Lage	Table	—	52	—	22.7	—	nr	—	35	—	nr	—	nr
Bigarella 1972 (p. 53, Table 5)	eolian	coastal dunes	modern	Itaperuba	Table	—	92	—	24.8	—	nr	—	37	—	nr	—	nr
Bigarella 1972 (p. 53, Table 5)	eolian	coastal dunes	modern	Laguna	Table	—	150	—	22.7	—	nr	—	41	—	nr	—	nr
Bigarella 1972 (p. 53, Table 5)	eolian	coastal dunes	modern	Camacho	Table	—	57	—	21.1	—	nr	—	33	—	nr	—	nr
Bigarella 1972 (p. 53, Table 5)	eolian	coastal dunes	modern	11 km NE of Balneario Jaguaruna	Table	—	36	—	19.4	—	nr	—	33	—	nr	—	nr
Bigarella 1972 (p. 53, Table 5)	eolian	coastal dunes	modern	Balneario Jaguaruna	Table	—	143	—	20.3	—	nr	—	34	—	nr	—	nr

Table 2, continued

Bigarella 1972 (p. 53, Table 5)	eolian	coastal dunes	modern	Balnerio Rincao	Table	—	100	—	18.6	—	nr	—	35	—	nr	—	nr
Bigarella 1972 (p. 53, Table 5)	eolian	coastal dunes	modern	Morro dos Conventos	Table	—	136	—	21.9	—	nr	—	37	—	nr	—	nr
Bigarella 1972 (p. 53, Table 5)	eolian	coastal dunes	modern	24 km SW of Morro dos Conventos	Table	—	34	—	23.6	—	nr	—	36	—	nr	—	nr
Bigarella 1972 (p. 53, Table 5)	eolian	coastal dunes	modern	Passo de Torres	Table	—	76	—	18.7	—	nr	—	32	—	nr	—	nr
Bigarella 1972 (p. 54, Table 6)	eolian	coastal dunes	modern	Torres north	Table	—	52	—	22	—	nr	—	36	—	nr	—	nr
Bigarella 1972 (p. 54, Table 6)	eolian	coastal dunes	modern	Torres south	Table	—	115	—	21.3	—	nr	—	35	—	nr	—	nr
Bigarella 1972 (p. 54, Table 6)	eolian	coastal dunes	modern	Praia da Figuerinha	Table	—	39	—	20.1	—	nr	—	34	—	nr	—	nr
Bigarella 1972 (p. 54, Table 6)	eolian	coastal dunes	modern	6.5 km NE Capao da Cauoa	Table	—	90	—	19.3	—	nr	—	34	—	nr	—	nr
Bigarella 1972 (p. 54, Table 6)	eolian	coastal dunes	modern	Tramandai	Table	—	125	—	18.3	—	nr	—	35	—	nr	—	nr
Bigarella 1972 (p. 54, Table 6)	eolian	coastal dunes	modern	Barro Preto	Table	—	51	—	18.7	—	nr	—	34	—	nr	—	nr
Bigarella 1972 (p. 54, Table 6)	eolian	coastal dunes	modern	Cidreia	Table	—	66	—	18.3	—	nr	—	31	—	nr	—	nr
Bigarella 1972 (p. 54, Table 6)	eolian	coastal dunes	modern	Pinhal north	Table	—	130	—	21.2	—	nr	—	32	—	nr	—	nr
Bigarella 1972 (p. 54, Table 6)	eolian	coastal dunes	modern	Pinhal south	Table	—	105	—	19.3	—	nr	—	37	—	nr	—	nr
Bigarella 1972 (p. 54, Table 6)	eolian	coastal dunes	modern	18 km south of Pinhal	Table	—	69	—	24.5	—	nr	—	46	—	nr	—	nr
Bigarella 1972 (p. 54, Table 6)	eolian	coastal dunes	modern	40 km south of Pinhal	Table	—	84	—	22	—	nr	—	36	—	nr	—	nr
Bigarella 1972 (p. 54, Table 6)	eolian	coastal dunes	modern	El Ppinar	Table	—	33	—	16.5	—	nr	—	36	—	nr	—	nr
Bigarella 1972 (p. 54, Table 6)	eolian	coastal dunes	modern	Km 79	Table	—	32	—	16.4	—	nr	—	35	—	nr	—	nr

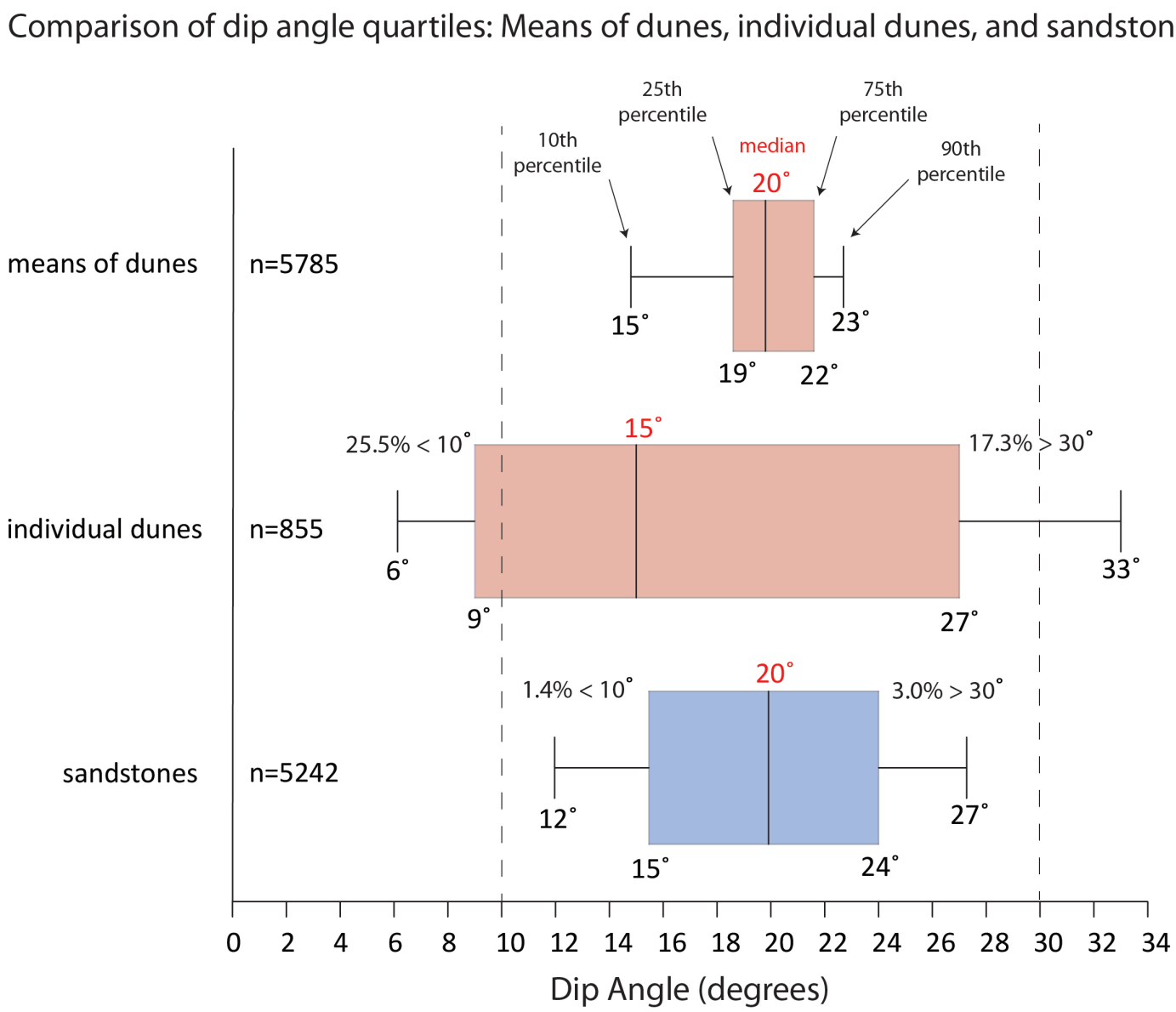

Fig. 6. A comparison of 5,785 points collected from the means of modern dunes, 855 dip measurements from modern dunes, and 5,242 dip measurements from sandstone cross-beds plotted as box plots. Most of the discussion in this paper centers around the "dunes" and "sandstones" data. Note that 25.5% of the dune data are less than 10°, and 17.3% of the data are greater than 30°. On the other hand, only 1.4% of the sandstone data are less than 10° and only 3.0% are greater than 30°.

C. Sandstones rarely have cross-bed inclinations < 10° and >30°; but they are common in eolian dunes

The results shown in Fig. 7 are consistent with the trends originally noted when comparing the Nebraska Sand Hills with the Coconino Sandstone (Fig. 3). Note that relatively low dips (<10°) and high dips (>30°) are uncommon in the sandstone data, but relatively common in the eolian dune data. Note that a full quartile of dune measurements (25th to 50th, 9-15° in the center plot of Fig. 6) falls below the lower quartile of the sandstone measurements (25th to 50th, 15-20°, bottom plot of Fig. 6). Note that half of the "dunes" measurements (center plot Fig. 6) fall below 15°, 10% fall below 6°, and 10% occur above 33°; whereas in sandstones only 10% of the measurements fall below 12° and only 10% are greater than 27°. Analyzed in another way, 25.5% of the eolian measurements are less than 10° while 17.3% of the measurements are greater than 30°. In sandstones, only 1.4% of the measurements are less than 10° while 3.0% of the measurements are greater than 30°.

D. Sandstone cross-bed dips are similar to each other, despite set thicknesses

Set thicknesses for beds and cross-beds have typically been defined as laminae (0-1 cm), very thin beds (1-3 cm), thin beds (3-10 cm), medium beds (10-30 cm), thick beds (30-100 cm), and very thick beds (>100 cm) (McKee and Weir 1953; Allen 1963; Boggs 2012). However, this classification scheme does not recognize size differences for cross-bed sets thicker than 1 meter. McKee and Bigarella frequently use the term "large" to describe thick sets of what

Table 3. A summary of the overall results when measuring dip angles of modern sand dunes and ancient sandstones.

	n	Mean (°)	Median (°)
Weighted means of dunes	5785	19.8	19.8
Dunes	855	17.8	15.0
Sandstones	5242	19.8	19.9

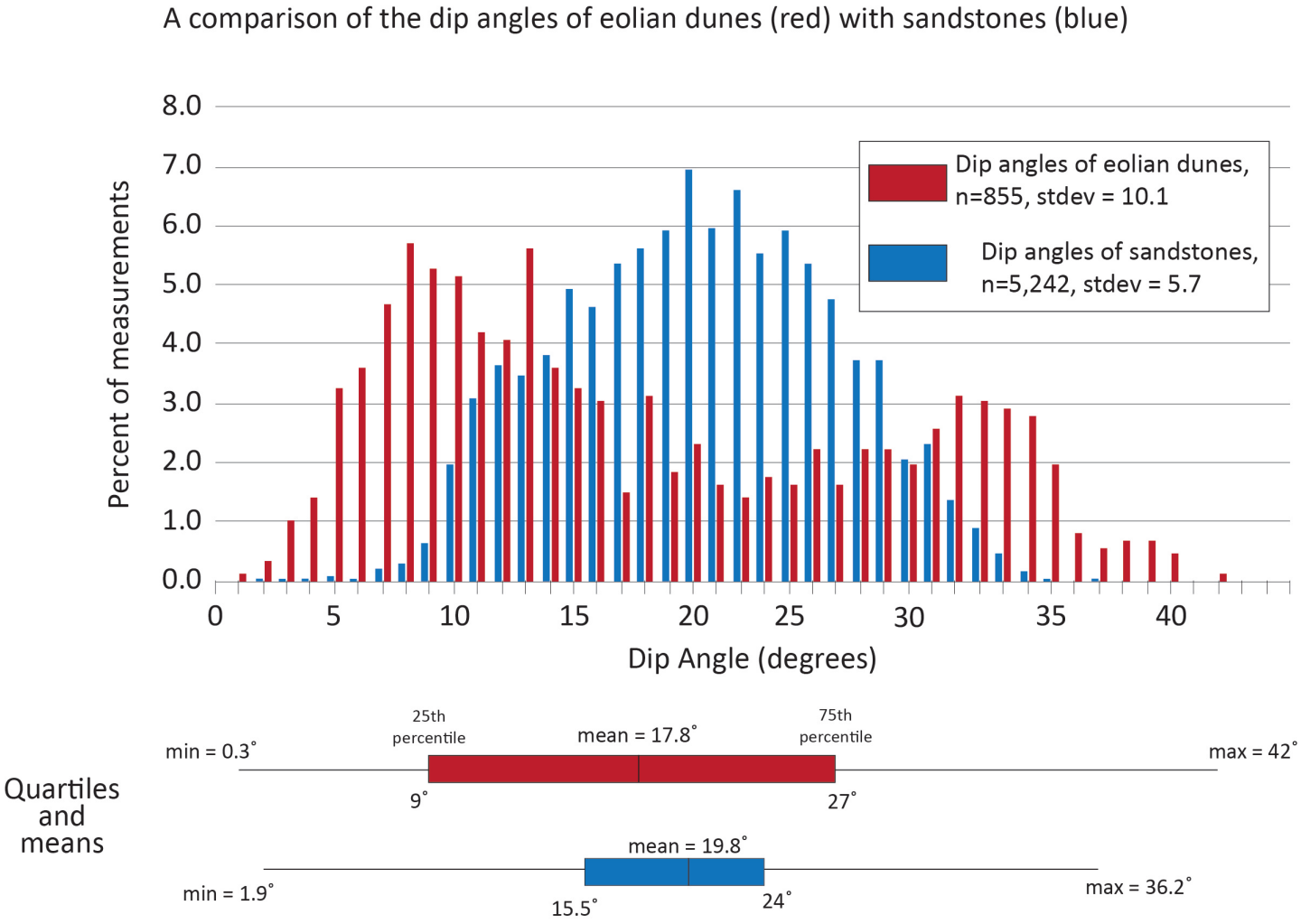

Fig. 7. A comparison of 855 dip measurements from modern dunes, and 5,242 dip measurements from individual sandstone cross-beds plotted as a histogram. Note the bimodal curve of the eolian dunes and the bell-shaped curve of the sandstones. Box plots of the data are plotted below the histogram. The greater spread of the eolian data are indicated by the greater standard deviation of the data (10.1) compared to the narrower distribution of the dune data and a smaller standard deviation (5.7). Most have focused on the larger number of high-angle cross-bed dips in eolian settings but note the even greater number of low-angle cross-bed inclinations. Sandstones are "compacted," while eolian dunes typically have porosities of about 40%. Some authors have suggested the sandstone data can be produced by "compacting" the eolian data by about 24% (see Fig. 10).

they believe to be eolian sandstones throughout their 1979a paper, but never seem to define or give reference to what "large" means. The author assumes that "large" is how McKee and Weir defined it in 1953 (>1.0 m), but this definition does not help distinguish between the thinner sets of cross-beds in the Coconino compared to the thicker ones the Navajo, for example.

Table 4 and Fig. 8 illustrate statistics for some sandstones with cross-bed set thicknesses that are either known from personal experience or have been reported in the literature. For this paper, small cross bed sets are defined as having a thickness of < 1.0 m, medium sets are defined as 1.0-5.0 m thickness, and large sets are defined as being thicker than 5.0 m. There are few data on set thicknesses, which can be highly variable in a sandstone, even with large, or thick (>5.0 m) cross-bed sets. As can be seen from Table 4 and Fig. 8, set thickness and dip angle do not appear to be related to each other. It is apparently an optical illusion that thicker sets appear to have steeper cross-bed dip angles.

E. Coconino, Wescogame, and Tapeats means cannot be differentiated

Using cross-bed dip data from Reiche (1938) and McKee (1940, 1982) a comparison was made between the Coconino, Tapeats, and Wescogame Sandstone means with Microsoft Excel ANOVA (Fig.

Table 4. Cross-bed set thickness compared to central tendencies and standard deviations of cross-bed inclinations for ancient sandstones. Note that the central tendencies are similar despite cross-bed set thickness. Assigned cross-bed set thicknesses are as follows: small (< 1.0 m), medium (1.0-5.0 m), and large (> 5.0 m). These data are shown graphically in Fig. 08.

Sandstone	Place	Reference for cross-bed angle measurements	Set thickness reference	Assigned set thickness	n	Mean cross-bed angle	Median cross-bed angle	Maximum cross-bed angle	Minimum cross-bed angle
Tapeats	Arizona	McKee 1940	McKee 1940, p. 818	small	183	20.3	20.9	27.9	4.8
Wingate	New Mexico	Reiche 1938	Clemmensen et al. 1989, p. 760	small	48	18.8	20.2	30	5.6
Cedar Mesa	Utah	Reiche 1938	Mountney and Jagger 2004	medium	67	18.7	18.5	33	5.7
Manakacha	Arizona	McKee 1982	McKee 1982, p. 216	medium	250	19.5	19.2	31.4	4.4
Esplanade	Arizona	McKee 1982	McKee 1982, p. 216	mostly medium	505	19.0	19.3	32.7	4.7
Wescogame	Arizona	McKee 1982	McKee 1982, p. 216	mostly medium	619	19.9	19.8	30.3	4.5
Coconino	Arizona	Reiche 1938	Whitmore (personal)	medium to large	197	20.3	20.8	33.8	4.7
Coconino	Arizona	Maithel 2019	Whitmore (personal)	medium to large	135	19.8	21.0	27	4.0
Coconino	Arizona	Whitmore unpubl	Whitmore (personal)	medium to large	214	20.2	21.0	32	5.7
De Chelly	Arizona	Reiche 1938	Whitmore (personal)	medium to large	82	21.5	22.8	33.4	5.0
Botucatú	Paraná, Brazil	Bigarella and Salamuni 1961	McKee and Bigarella 1979a	large	626	19.5	19.1	33.3	6.2
Botucatú	Rio Grande do Sul, Brazil	Bigarella and Salamuni 1961	McKee and Bigarella 1979a	large	598	20.5	20.2	32.5	6.2
Botucatú	São Paulo, Brazil	Bigarella and Salamuni 1961	McKee and Bigarella 1979a	large	650	20.1	20.0	32.5	6.2
Casper	Wyoming	Fryberger et al 2016	personal (2011)	large	18	20.1	22.0	27	4.5
Navajo	Utah	Reiche 1938	McKee and Bigarella 1979a, p. 212	large	33	22.1	23.1	36.2	5.4
Navajo	Utah	Kiersch 1950	McKee and Bigarella 1979a, p. 212	large	229	17.2	18.5	31.2	5.3
Navajo	Utah	Whitmore unpubl	McKee and Bigarella 1979a, p. 212	large	44	21.5	23.0	26.0	3.8
Tensleep	Wyoming	Fryberger et al 2016	Kerr and Dott 1988, p. 389	large	47	21.1	22.0	34	5.1

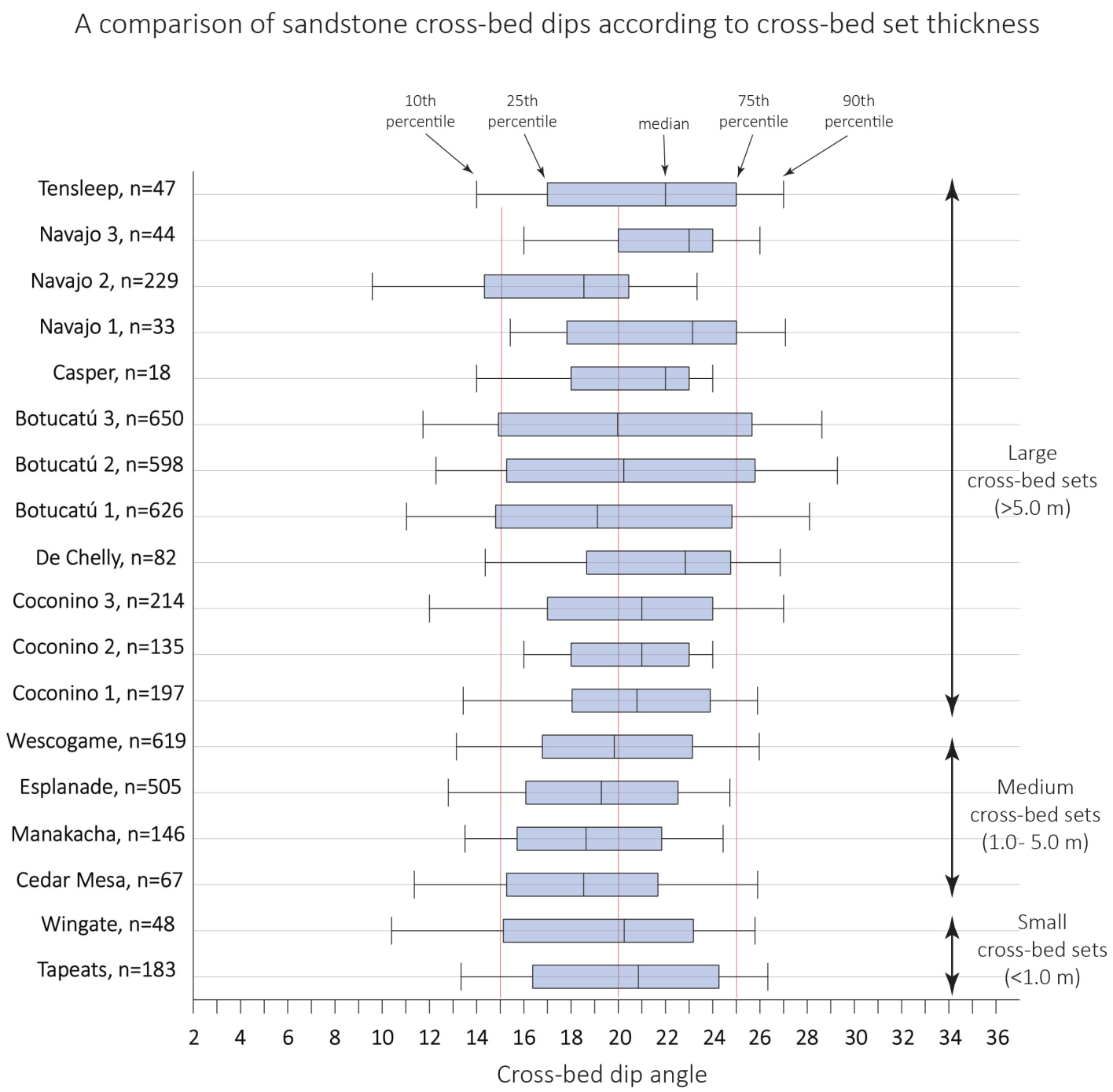

Fig. 8. A comparison of sandstone cross-bed inclinations arranged by set thickness. Small (thinner) cross-bed sets are at the bottom and larger (thicker) cross-bed sets are at the top. "Steep" cross-beds in thick sets are apparently an optical illusion. Compare the small sets of the Tapeats with the thick sets of the Navajo.

9). McKee identified the depositional environment of the Coconino as eolian (1934), the Tapeats as shallow marine (1945), and the Wescogame as fluvial (1982). The analysis showed that there is no statistically significant difference between the sets of data (p=0.75), despite the three formations having different cross-bed set thicknesses (Fig. 8) and different supposed depositional environments.

IV. DISCUSSION

A. Limitations of the data set

The data set is certainly not perfect. Although many of my dune data points come from weighted means, much of that data was not used in the comparisons because it was not collected in the same

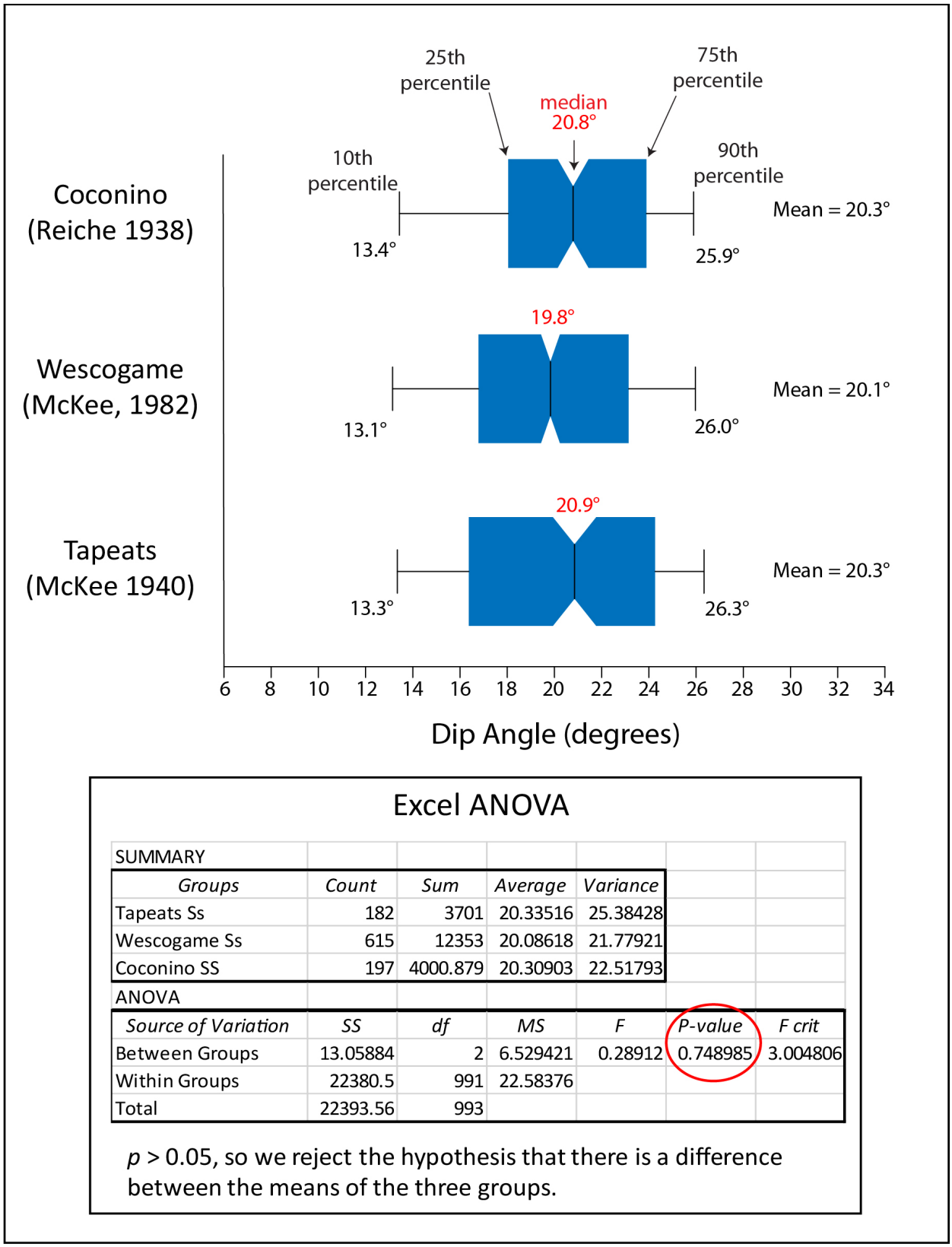

Excel ANOVA

SUMMARY

Groups	*Count*	*Sum*	*Average*	*Variance*
Tapeats Ss	182	3701	20.33516	25.38428
Wescogame Ss	615	12353	20.08618	21.77921
Coconino SS	197	4000.879	20.30903	22.51793

ANOVA

Source of Variation	*SS*	*df*	*MS*	*F*	*P-value*	*F crit*
Between Groups	13.05884	2	6.529421	0.28912	0.748985	3.004806
Within Groups	22380.5	991	22.58376			
Total	22393.56	993				

$p > 0.05$, so we reject the hypothesis that there is a difference between the means of the three groups.

Fig. 9. A comparison of three sets of data from cross-bedded sandstones of the Grand Canyon area in the form of notched box plots. The "notch" indicates the 90% confidence interval for the mean. The Coconino consists of 197 measurements from Reiche (1938), the Wescogame 615 measurements from McKee (1982), and the Tapeats 182 measurements from McKee (1940). Analysis with Excel ANOVA showed that the three data sets could not be statistically distinguished from one another. This is despite varying cross-bed set thickness (Coconino, large; Wescogame, medium; Tapeats, small) and supposed depositional environment (Coconino, eolian; Wescogame, fluvial; Tapeats, shallow marine).

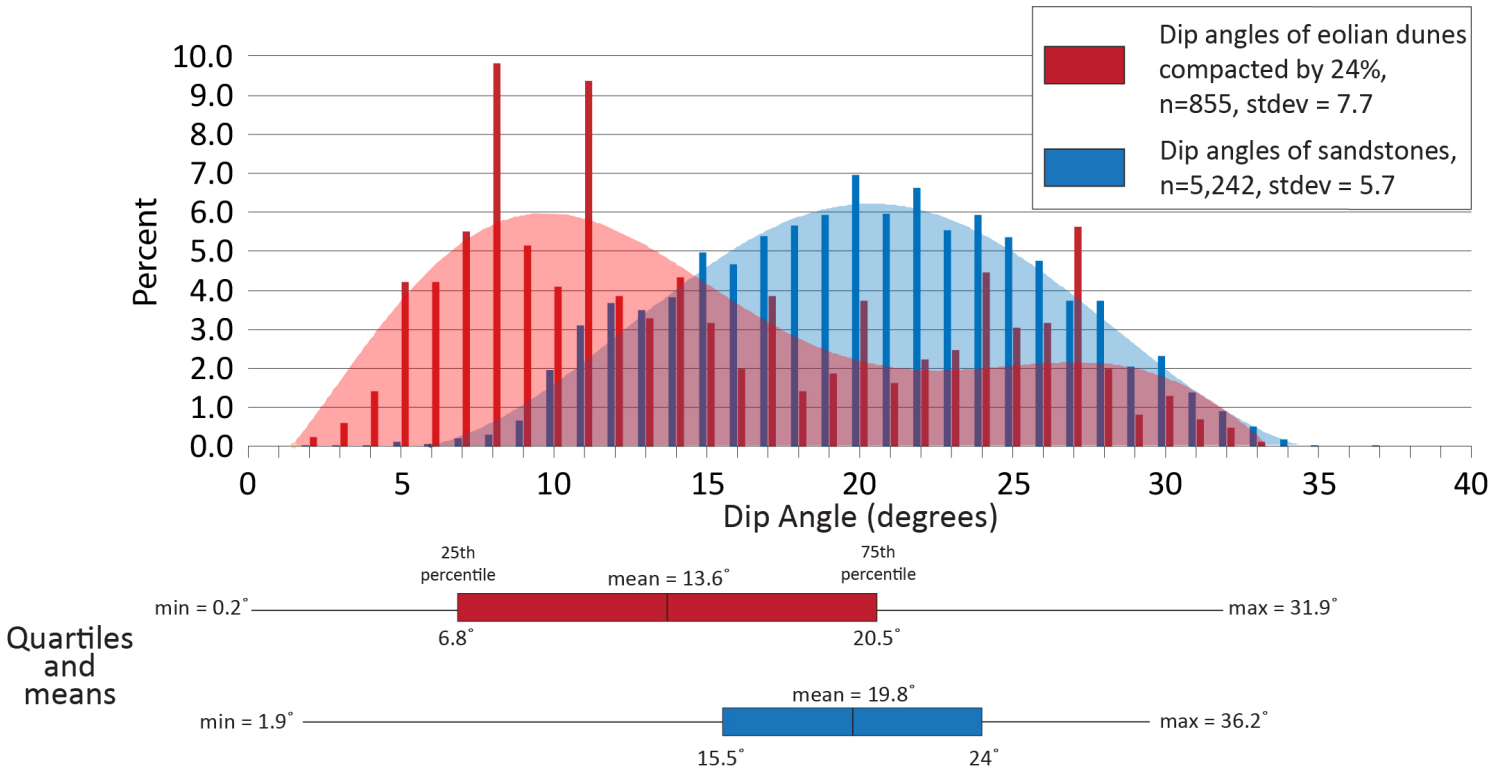

Fig. 10. A comparison of cross-bedded sandstone dip angles with "compacted" eolian dip angles (compare Fig. 7). The claim is often made that supposed eolian cross-bedded sandstones lack steep dip angles because the eolian sands have been compacted, lowering the dip angles by about 24% (according to Corey et al. (2005) and Walker and Harms (1972)). To test whether this is a reasonable hypothesis or not, each eolian dip from Fig. 7 was compacted 24% and then re-plotted with the sandstone dips to get an approximation of what the compacted dune angles would look like. Steeper cross-bed dips would be more affected than shallower ones. The result shows the two distributions do not match. A reasonable conclusion is that cross-bedded sandstones could not have been derived from compacted eolian dunes. In the past, most workers have focused on the average angle or the missing steep angles in sandstones. However, this distribution shows an even bigger problem: the missing shallow angles in sandstones. Note the bell-shaped curve of the sandstones. The eolian dune curve has become, more or less, a bell-shaped curve that is skewed to the right. It has largely lost the bimodality seen in Fig. 7. The curves were generated with Microsoft Excel using a 6th-order polynomial trendline fit. The R2 value for the sandstones was 0.98 and 0.66 for the compacted eolian dunes. The ends of the curves were truncated, as they contained some negative values and were beyond the set of data.

way as many of the sandstone measurements. Much other data were found but could not be used because it was reported in the form of histograms, like the Nebraska Sand Hills data (Ahlbrandt and Fryberger 1980). The data points in both sets probably could have been doubled if individual measurements had been reported. When individual measurements were reported, sometimes the plots were not sharp and there was some overlap of the points. It is not known from any of the sets whether the data were collected randomly, if every accessible point was collected, or if some data were ignored in favor of collecting easier measurements. This might have been especially true of the dune data because avalanching occurs so readily on steeper slopes. When collecting my data from sandstones, I always tried to spread out my measurements over a wide area, trying to collect reliable data from all exposed cross-bed sets. In particular, I looked for flat, well-exposed foresets from which I could obtain reliable measurements. I tried not to ignore steep cross-beds or shallow ones, trying to make my measurements a representative sample of the exposures. Attempts were made not to repeat measurements on the same foresets. The assumption was made that other workers collected their data in much the same way that I did (authors almost never give precise details on how they make their strike and dip measurements).

It is noteworthy that much of the data in this report (both sandstone and dune) were collected by Edwin McKee and his associates (like João Bigarella) who were firmly convinced of the eolian origin of sandstones like the Coconino and Navajo (see McKee and Bigarella 1979a). If someone was biased toward an eolian origin of a particular sandstone, they might tend to collect steeper dips over shallower ones. However, I am encouraged that my Coconino data set compared very favorably with that of Reiche (1938) and Maithel (2019), possibly indicating that the data in these three cases were consistently collected, despite philosophical differences. It is curious that McKee never reported any detailed data of his own Coconino cross-bed inclinations despite writing the first detailed paper on the Coconino (1934); using the Coconino as a "type" example of an eolian sandstone (McKee and Bigarella 1979a); and publishing extensive data on cross-bed inclinations of other formations, primarily in the Grand Canyon area (1940, and 1982). McKee seemed to ignore the data of Reiche (1938) when he reported the cross-bed inclinations in the Coconino were "mostly at 25-30°, but a few reach a maximum of 34°" (McKee and Bigarella 1979a, p. 199), although he was certainly aware of Reiche's work (1940, p. 812).

B. Based on the data, compaction/erosion cannot explain the differences in dip angles between dunes and sandstones

Some have recognized that supposed eolian sandstones lack cross-bed inclinations which are at the angle of repose; this is refreshing considering how many claims there are to the contrary. Authors have appealed to post-depositional compaction to explain the reduction of cross-bed inclinations (Corey et al. 2005; Glennie 1972, p. 1058; Hunter 1981, p. 323; McKee and Bigarella 1979a, p. 191, 218; Rittenhouse 1972; Walker and Harms 1972, p. 280). Walker and Harms calculated (p. 280) that if cross-bedded sand at the angle of repose (34°), had an initial porosity of 40% and was compacted down to 20% porosity, the angle would become about 27°, or an angle reduction of about 24%. Corey et al. found a similar value and claimed compaction and cement production could reduce angles from 32° to 24° in the Navajo Sandstone (24° was their average (compacted) angle measurement).

Our calculations (Emery et al. 2011) showed that angle reduction probably happened, but only by a few degrees. The work in that abstract was preliminary and needs to be further developed. However, based on hundreds of thin sections that we examined from the Coconino, we found very little evidence for significant compaction. We looked for things like fractured grains, deformed ooids, and bent muscovite flakes, all of which were largely lacking from the Coconino and shows that an initial porosity of 40%, similar to eolian dunes, which is unreasonable.

Missing higher angles have also been attributed to the erosion and non-preservation of the uppermost part of the foreset beds (where the angles are usually the steepest) being eroded away and not preserved (Collins 2022, McKee and Bigarella 1979a, p. 218; Poole 1962, p. D148; Walker and Harms 1972, p. 280). It is well-known that the steepest parts of eolian dunes are on the upper part of the foreset slope, just below the crest (Hunter 1977).

When making comparisons of cross-bed angles in supposed eolian sandstones to modern eolian dunes, the focus has always been on high angles, missing high angles, or the average. However, this study has uncovered a major oversight in comparing sandstone cross-bed angles with modern dunes. The low-angle dips missing from the sandstones and abundantly present in modern dunes have been overlooked (examine Fig. 6). More than 25% of modern dune angles are less than 10%, compared to only 1.4% of sandstones. If the sandstones have been compacted, the low dip angles should still be there; but they are missing. Examining the two sets of data using quartiles and standard deviations (Fig. 7) shows that the cross-bed dip data of sandstones and modern eolian dunes that can be clearly distinguished. The sandstone cross-bed data set cannot be achieved by compacting the modern eolian dune set; it would not produce the low angles so abundant in the dune data set. Considering Fig. 7, note that the dune set is bimodal, compared to the more normal distribution of the sandstone dip angles; compacting the dune set would not give the same distribution as the sandstone set—there would be even more low angles (note that the sandstone set is already "compacted"). A similar problem occurs by claiming that the higher angles were just eroded away and that is why they are not preserved. Erosion of the tops of the dune sets would still preserve the lower parts of the dunes that contain the low angles.

To help illustrate this problem, Fig. 10 was drafted. Consistent with what Corey et al. (2005) and Walker and Harms (1972) proposed, each of the initial 855 dune measurements was compacted 24% and then re-plotted. One can see that compacting the dune data does not produce the sandstone data. Not only do the higher dune angles of the compacted dunes not "catch up" to the percentages found in the sandstones (compare the blue and red shading on the right side of the plot), but now there are even more low angles in the dune data (on the left side of the plot). Note that the dune data nearly loses its bimodality and becomes, more or less, a normal curve that is skewed to the right. The methods of making this curve are more fully described in the figure caption.

One may argue that the current dune data set of individual measurements are primarily from the coastal dunes in Brazil and the gypsum dunes of New Mexico, which may not be quite analogous to depositional environments of sandstones like the Coconino or Navajo. It is not that no measurements were made in other locations, it is simply the type of data that are available from these other locations. The plots of the Nebraska Sand Hills (Fig. 3), an inland sand sea, could similarly be compacted, and the results would be the same with an abundance of low angles.

C. Is "steep" an optical illusion if cross-bed sets are thick?

I have often asked groups of people standing with me around cross-bedded sandstones to estimate the angle of the cross-beds for me. Inevitably, when cross-bed sets are thick higher angles are guessed and when cross-bed sets are small, lower angles are anticipated. All are usually surprised when I demonstrate the dip angle with a Brunton compass or, more recently an iPhone. I have made the same observation from the literature. Never have I read about the Tapeats Sandstone (with small cross-bed sets) having "angle of repose dips" or even "steep" dips. However, descriptions of sandstones with thicker cross-bed sets like those of the Coconino, or especially the Navajo, abound with descriptors like "angle of repose," "steep," or "steeply inclined" even though these sandstones have average angles that are very close to one another (Fig. 8). The only conclusion that I have been able to reach, is that observers are often fooled into thinking that thicker sets of cross-beds have steeper angles. As scientists, we should always fall back on data to back up our claims. Even Edwin McKee himself seems to have fallen to this illusion. In his 1940 paper, where he published the Tapeats Sandstone data used in this paper, he has an interesting discussion of how much steeper the Coconino cross-beds are than the Tapeats cross-beds (p. 823), where, as this paper has shown, the two sets of data cannot be statistically distinguished from one another (Fig. 9)!

D. Are average cross-bed inclinations in eolian dunes less than cross-bedded sandstones?

An unexpected result of this study is the conclusion that eolian cross-beds may have (on average) shallower cross-bed dips than cross-bedded sandstones. An examination of Fig. 6 shows that dunes have an average of 15° compared to 20° for sandstones. Again, this is a surprising result because most people have focused on the steep dips for modern dunes and have ignored the abundance of shallow dips that are also present.

E. Are any cross-bedded sandstones eolian?

In this paper, two sets of cross-bed dip angle data were considered: those from modern dunes and those from sandstones. The study was initially conducted to compare the cross-bed dips of the Coconino with modern eolian dunes. The study was extended to include other sandstones. The data shows that all of the sandstones examined have similar means, but very different distributions when considering the complete set. Especially telling is the abundance of low cross-bed dips in modern dunes and the differences in the standard deviations of cross-bed angles between sandstones and dunes. All of the sandstones examined have narrow standard deviations and a lack of low dip angles when compared to dunes, showing the sandstones can be clearly distinguished from the modern dunes and that the sandstones probably all formed in similar non-eolian settings. Whitmore and Garner (2018) showed that many characteristics of the Coconino were non-eolian in origin; this study shows one more non-eolian characteristic that is not only applicable to the Coconino, but a host of other sandstones as well.

F. Future work

To corroborate the conclusions of this paper, more dune measurements need to be made in large dune fields. Current technology may be able to help in getting an almost infinite number of accurate slope measurements. Hi resolution lidar imagery could be used with programs like ArcGIS to calculate dune slopes in specific areas with a grid overlay. An approach like this would help eliminate bias. I predict this approach will not radically change the data in this paper, but nonetheless, the approach should be tried.

V. CONCLUSION

In consideration of more than 6,000 cross-bed inclinations of modern dunes and more than 5,000 inclinations of sandstones, many of which are supposed eolian deposits, it is concluded that measurements reported from modern eolian dunes do not compare well with their supposed counterparts in the rock record. Most creationists have thought that eolian cross-bed dips are steeper and water-laid cross-bed sets are shallower. This is not exactly true, or a good way to characterize the differences. Although central tendencies of the two sets of data are similar, the standard deviation of dune measurements is 10.1 compared to the standard deviation of sandstone measurements which is lower at 5.7, meaning the sandstone data are more "bunched" together (Fig. 7). Most significantly, 25.5% of the dune data measurements are less than 10°, where only 1.4% of the sandstone data are less than 10°. 17.3% of the dune data are greater than 30°, whereas only 3.0% of the sandstone data are greater than this value (Fig. 6). Sedimentary compaction and erosion of steeper angles near the top of the foresets have usually been cited as the reasons for this discrepancy. Some lowering of cross-bed dip values certainly occurs by this mechanism as porosity is reduced, but the reduction of dips cannot explain the near absence of low cross-bed dips in sandstones. My data clearly show that modern eolian cross-bed dips cannot produce the collection of cross-bed dips that we see in ancient sandstones (Fig. 10). Additionally, when individual sets of ancient sandstone cross-bed sets are compared, like the Coconino, Wescogame, and Tapeats of the Grand Canyon, the groups cannot be statistically differentiated (Fig. 9), despite their supposed different depositional environments and cross-bed set thicknesses. Considering cross-bed set thickness alone is not a reliable way to determine the depositional environment, as many have done. Sets of cross-bed inclination angles may be a more reliable way to help determine the depositional environment. Eolian cross-bed angles have a wide spread ranging from 0-40° and a standard deviation of about 10 (Fig. 7). None of the ancient sandstone data that was examined in this study matched those parameters, suggesting the sandstones in this study did not form in eolian settings.

ACKNOWLEDGEMENTS

The author would like to thank Cedarville University which has supported my work for many years. Several reviewers suggested changes that corrected errors and helped improve this paper. I appreciate their input and their time spent with this paper. Any errors remaining are my responsibility.

REFERENCES

Ahlbrandt, T.S., and S.G. Fryberger. 1980. Eolian deposits in the Nebraska Sand Hills. U.S. Geological Survey Professional Paper 1120A:1–24.

Allen, J.R.L. 1963. The classification of cross-stratified units, with notes on their origin. Sedimentology 2:93-114.

Allen, J.R.L. 1970. The avalanching of granular solids on dune and similar slopes. The Journal of Geology 78:326-351.

Bigarella, J.J. 1972. Eolian environments: Their characteristics, recognition and importance. In: J.K. Rigby and W.K Hamblin (editors), Recognition of Ancient Sedimentary Environments, pp. 12-62.

Bigarella, J.J., and R. Salamuni. 1961. Early Mesozoic wind patterns as suggested by dune bedding in the Botucatú Sandstone of Brazil and Uruguay. Geological Society of America Bulletin 72:1089-1106.

Bigarella, J.J., R.D. Becker, and G.M. Duarte. 1969. Coastal dune structures from Paraná (Brazil). Marine Geology 7:5-55.

Boggs. S., Jr. 2012. Principles of Sedimentology and Stratigraphy, 5th ed. New York: Pearson Prentice Hall.

Carrigy, M.A. 1970. Experiments on the angles of repose of granular material. Sedimentology 14:147-158.

Collins, L.G. 2022. Eolian or water deposition of the Coconino Sandstone. Retrieved December 29, 2022, from https://www.csun.edu/~vcgeo005/Nr91Eolian.pdf.

Corey, M.A., B.M. Simonson, and D.B. Loope. 2005. Physical compaction as a cause of reduced cross-bed dip angle in the Navajo Sandstone. Geological Society of America Abstracts with Programs 37(7):254.

Emery, M., S. Maithel, and J.H. Whitmore. 2011. Can compaction account for lower-than-expected cross-bed dips in the Coconino Sandstone (Permian), Arizona? Geological Society of America Abstracts with Programs 43(5):430.

Fryberger, S.G., N. Jones, M. Johnson, and C. Chopping. 2016. Stratigraphy, exploration and EOR potential of the Tensleep/Casper Formations, SE Wyoming. Search and Discovery Article #10851. Wyoming Geological Association, Casper, Wyoming.

Glennie, K.W. 1972. Permian Rotliegendes of northwest Europe interpreted in light of modern desert sedimentation studies. Bulletin of the American Association of Petroleum Geologists 56:1048-1071.

Hill, C., G. Davidson, T. Helble, and W. Ranney, (editors). 2016. The Grand Canyon Monument to an Ancient Earth. Grand Rapids, Michigan: Kregel Publications.

Hunter, R.E. 1977. Basic types of stratification in small eolian dunes. Sedimentology 24:361-387.

Hunter, R.E. 1981. Stratification styles in eolian sandstones: Some Pennsylvanian to Jurassic examples from the western interior U.S.A. In F.G. Ethridge, and R.M. Flores (editors), Recent and Ancient Nonmarine Depositional Environments: Models for Exploration, pp. 315-329. Tulsa, Oklahoma: Society of Economic Paleontologists and Mineralogists, Special Publication 31.

Hunter, R.E. 1985. Subaqueous sand-flow cross-strata. Journal of Sedimentary Petrology 55: 886-894.

Kerr, D.R., and R.H. Dott. 1988. Eolian dune types preserved in the Tensleep Sandstone (Pennsylvanian-Permian), north-central Wyoming. *Sedimentary Geology* 56:383-402.

Kiersch, G.A. 1950. Small-scale structures and other features of Navajo Sandstone, northern part of San Rafael Swell, Utah. Bulletin of the American Association of Petroleum Geologists 34:923-942.

Maithel, S.A. 2019. Characterization of Cross-Bedded Depositional Processes in the Coconino Sandstone. Loma Linda, California: Loma Linda University [Dissertation].

Maithel, S.A., L.R. Brand, and J.H. Whitmore. 2021. Characterization of hard-to-differentiate dune stratification types in the Permian Coconino Sandstone (Arizona, USA). Sedimentology 68:238-265. doi: 10.1111/sed.12774.

McKee, E.D. 1940. Three types of cross-lamination in Paleozoic rocks of northern Arizona. The American Journal of Science 238:811-824.

McKee, E.D. 1966. Structures of dunes at White Sands National Monument, New Mexico (and a comparison with structures of dunes from other selected areas). Sedimentology 7:1-69.

McKee, E.D. 1982. The Supai Group of the Grand Canyon. Washington, D.C.: United States Geological Survey Professional Paper 1173.

McKee, E.D., and G.W. Weir. 1953. Terminology for stratification and cross-stratification in sedimentary rocks. Bulletin of the Geological Society of America 64:381-390.

McKee, E.D., and J.J. Bigarella. 1979a. Ancient sandstones considered to be eolian. In E.D. McKee (editor), A Study of Global Sand Seas, pp. 187-238. U.S. Geological Survey Professional Paper 1052.

McKee, E.D., and J.J. Bigarella. 1979b. Sedimentary structures in dunes. In E.D. McKee (editor), A Study of Global Sand Seas, pp.83-134. U.S. Geological Survey Professional Paper 1052.

Middleton, L.T., D.K. Elliott, and M. Morales. 2003. Coconino Sandstone. In S.S. Beus and M. Morales (editors), Grand Canyon Geology, 2nd edition, pp. 163-179. New York: Oxford University Press.

Mountney, N.P., and A. Jagger. 2004. Stratigraphic evolution of an aeolian erg margin system: The Permian Cedar Mesa Sandstone, SE Utah, USA. *Sedimentology* 51:713-743.

Poole, F.G. 1962. Wind directions in late Paleozoic to middle Mesozoic time on the Colorado Plateau. U.S. Geological Survey Professional Paper 450D:147-151, article 163.

Reiche, P. 1938. An analysis of cross-lamination the Coconino Sandstone. Journal of Geology 46(7):905-932.

Rittenhouse, G. 1972. Cross-bedding as a measure of sandstone compaction. Journal of Sedimentary Petrology 42(3):682-683.

Snelling, A.A. 2021. The petrology of the Tapeats Sandstone, Tonto Group, Grand Canyon, Arizona. Answers Research Journal 14:159-254.

Strahler, A.N. 1999. Science and Earth History — The Evolution/Creation Controversy. Amherst, New York: Prometheus Books.

Thomas, B. 2021. New evidence of Flood in Grand Canyon. Institute for Creation Research. Retrieved December 29, 2022, from https://www.icr.org/article/13180.

Thomas, B., and T. Clarey. 2021. Zion National Park: Evidence of deep water sand waves. Institute for Creation Research Acts and Facts. Retrieved December 29, 2022, from https://www.icr.org/article/12778.

Walker, T.R. and J.C. Harms. 1972. Eolian origin of flagstone beds, Lyons Sandstone (Permian), type area, Boulder County, Colorado. Mountain Geologist 9:279-288.

Whitmore, J.H. 2019. Lithostratigraphic Correlation of the Coconino Sandstone and a Global Survey of Permian "Eolian" Sandstones: Implications for Flood Geology. Answers Research Journal 12:275-328.

Whitmore, J.H. 2021a. A comparison of dip angles from ancient cross-bedded sandstones and modern eolian dunes. Geological Society of America Abstracts with Programs 53(6). doi: 10.1130/abs/2021AM-369476.

Whitmore, J.H. 2021b. An analysis of the inclination (dip) of cross-bedded sandstone units. Journal of the Creation Theology and Science Series C: Earth Sciences 11:3.

Whitmore, J.H., and P.A. Garner. 2018. The Coconino Sandstone (Permian, Arizona, USA): Implications for the origin of ancient cross-bedded sandstones. In J.H. Whitmore (editor), Proceedings of the Eighth International Conference on Creationism, pp. 581–627. Pittsburgh, Pennsylvania: Creation Science Fellowship.

Young, D.A., and R.F. Stearley. 2008. The Bible, Rocks and Time. Downers Grove, Illinois: InterVarsity Press.

THE AUTHOR

Dr. John H. Whitmore currently serves as Senior Professor of Geology at Cedarville University where he has been teaching since 1991 and started a young earth geology major in 2009 which has now produced more than 50 graduates. He is closely associated with Canyon Ministries and Answers in Genesis who sponsor annual raft trips in the Grand Canyon for which John teaches the geology. He has written widely, especially about the Coconino Sandstone. He served as editor of the ICC Proceedings in 2018 and 2023.